学位論文

Moderately Chaotic Hamiltonian Systems: Structure and Motion in High-dimensional Phase Spaces (中間カオスハミルトン系：高次元相空間における構造と運動)

１９９７年

山口義幸

Moderately Chaotic Hamiltonian Systems: Structure and Motion in High-dimensional Phase Spaces

YAMAGUCHI Y. Yoshiyuki [1]
Department of Physics, School of Science, Nagoya University,
Furo-cho, Chikusa-ku, Nagoya, 464-01, Japan

[1]e-mail: yamaguchi@allegro.phys.nagoya-u.ac.jp

The Construction of this Thesis

This thesis is constructed from seven chapters. Chapter 1 is for introduction. Chapter 2 is a review of Hamiltonian dynamical systems, and some theorems for chaotic systems are shown. This chapter will help the readers to understand what have been known and what are new in my own works. Chapters 3-6 are for my original works. Chapter 7 is devoted for summary and discussions.

The heart of this thesis is to understand the global structure of phase space in Hamiltonian systems with many degrees of freedom. Such systems includes a new class which is different from the ones proposed up to now, and I introduce the class as moderately chaotic systems. In chapter 5 I investigate properties of the class, and I construct a geometrical model of phase space in chapter 6 by using results obtained in chapter 5. The two chapters are the main parts of this thesis.

Most of the content of chapters 4 appeared in the articles [Yam96] and [Yam97], and of chapters 5 and 6 appeared in [Yam98] and [YK98a] respectively.

Acknowledgement

I express my thanks to Tetsuro Konishi for valuable discussions and careful reading of the manuscript. Careful progress of the discussions stimulated me tending to rush to conclusions. Most of the content of this thesis has been made through the discussions.

I am also grateful to Hiroyasu Yamada for helpful discussions. His deep knowledge covering wide fields and persistent discussions always gave me useful comments. It is great happiness for me that he was one of my roommates.

I thank the Computer Center of the Institute for Molecular Science, for the use of the NEC SX-3/34R.

I also acknowledge to the following people for fruitful discussions and helpful advices: Satoru Kurosaki, Yasushi Shimizu, Kazuo Kitahara, Shin-ichi Sasa, Tatsuo Yanagita, Shinji Takesue, Naoko Nakagawa, Kunihiko Kaneko, Ichiro Tsuda, Chihiro Seko, Shogo Tanimura, Kouji Nakamura, Ryo Akiyama, Akira Yoshimori, Yasusada Nambu, Atsushi Taruya, Kenji Imai, Masaharu Ishii, Kazuhiro Nozaki and members of R-lab. at Nagoya university.

Contents

Chapter 1

Introduction

The studies of classical dynamics have started from Newton in the 17th century, and the dynamics is one of powerful tools to study temporal evolutions of nature. We are particularly interested in Hamiltonian dynamical systems with many degrees of freedom because they show interesting phenomena, for instance, cooperative phenomena like phase transition.

Dynamical systems are generally chaotic, and hence we need to know what is chaos. In Sec.1.1 we shortly review regular and chaotic motions and their properties. One of the features of chaotic motion is to lose initial information exponentially, and chaotic motion is unpredictable accordingly.

In spite of the exponential loss, long time tail often appears in chaotic systems. The long time tail is described in Sec.1.2, and we reach the understanding that we must focus on global structure of phase space, on which we usually consider dynamical systems.

In Sec.1.3 we review global structures for the three classes of Hamiltonian systems: integrable, nearly integrable and fully chaotic systems, whose details are described in Chap.2. Hamiltonian systems are usually classified into the three classes.

However, in systems with many degrees of freedom, there is a phenomenon which occurs in a new class differing from the three classes. We therefore introduce the new class as moderately chaotic systems in Sec.1.4. One of the main purposes of this thesis is to reveal the global structure of phase space in moderately chaotic systems with many degrees of freedom.

1.1 Regular and chaotic motions

In this section we review properties of regular and chaotic motions with the three ways: times series, power spectra and Lyapunov exponent.

1.1.1 Time series

Let us show examples of regular and chaotic motions. We consider the following Hamiltonian system,

$$H(q,p) = \frac{1}{2}(p_1^2 + p_2^2) + (1 - \cos q_1) + \frac{1}{2}q_2^2 + \epsilon(1 - \cos q_1)q_2. \qquad (1.1)$$

Two regular and two chaotic orbits are shown in Figs.1.1(a) and (b), respectively. Initial conditions of the two orbits are slightly different from each other. The two regular orbits are periodic and keep the initial difference. On the other hand, the two chaotic orbits, $q_1(t)$ and $q_1'(t)$, are rather complex and the initial difference grows and becomes visible although it is extremely small at the initial time. The initial difference is regarded as error of observation of initial condition, which is essentially not avoidable, and the error exponentially grows with the passage of the time between the chaotic orbits as shown in Fig.1.2, i.e.

$$\Delta q_1(t) \equiv |q_1(t) - q_1'(t)| \propto \mathrm{e}^{\lambda t}, \qquad \lambda > 0. \qquad (1.2)$$

The sensitivity to initial condition is one feature of chaotic motion, and hence chaotic motion is unpredictable although system is deterministic. The motion is therefore called deterministic chaos. A dynamical system is deterministic if the state in the future is uniquely determined once an initial condition is determined. Systems defined by ordinary differential equations without noise are deterministic, and systems following stochastic differential equations as Langevin equations are not deterministic.

1.1.2 Lyapunov exponent

We usually use the (largest) Lyapunov exponent λ_1 to check whether an orbit is chaotic or not. The Lyapunov exponent measures separation of nearby orbits whose displacement is initially infinitesimal. Let $\delta x(t)$ be the displacement in phase space, then λ_1 is roughly defined as

$$|\delta x(t)| \sim |\delta x(0)| \exp(\lambda_1 t) \quad \text{as } t \to \infty. \qquad (1.3)$$

When $\lambda_1 > 0$ slight difference of initial condition grows, and accordingly, the orbit is unpredictable and chaotic. In Fig.1.3 we show the difference of Lyapunov exponents between the regular and the chaotic orbits shown in Fig.1.1. Lyapunov exponent for the regular orbit converges zero and one for the chaotic orbit converges a positive value. See Appendix A for details of Lyapunov exponent.

1.1.3 Power spectra

Observing power spectrum is another method to distinguish chaotic motion from regular one. Figure 1.4 shows power spectra for regular and chaotic orbits shown

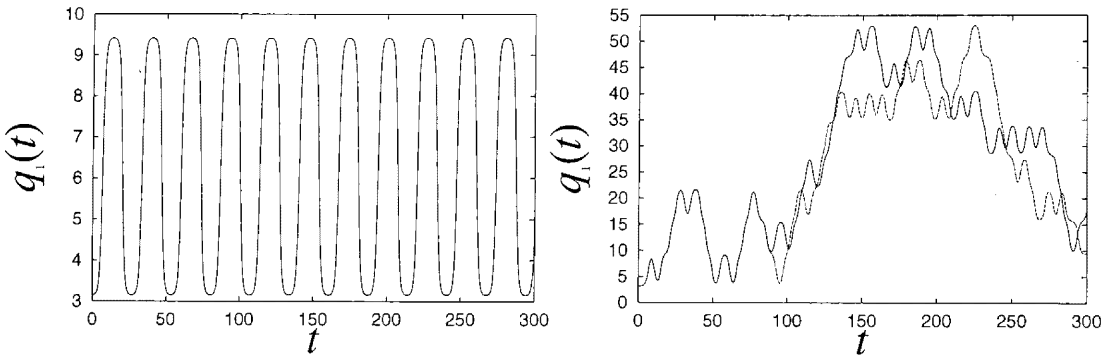

(a) Regular orbits (b) Chaotic orbits

Figure 1.1: Regular and chaotic motion in the system (1.1). In each figure two orbits are shown whose initial conditions are slightly different from each other. The initial conditions except for p_2 are $p_1(0) = 0, q_1(0) = 3.151593$ and $q_2(0) = 0.1$ for an orbit and $q_2(0) = 0.100001$ for the other one. The total energy is $E = 5.5$. (a) Regular orbits. $\epsilon = 0$. $p_2(0) = 2.643880$ (b) Chaotic orbits. $\epsilon = 0.1$. $p_2(0) = 2.636304$. Regular orbits behave periodically and the difference between the two orbits keeps the initial one which is invisible. On the other hand, behaviours of chaotic orbits are complex and the difference becomes to be visible around $t = 100$.

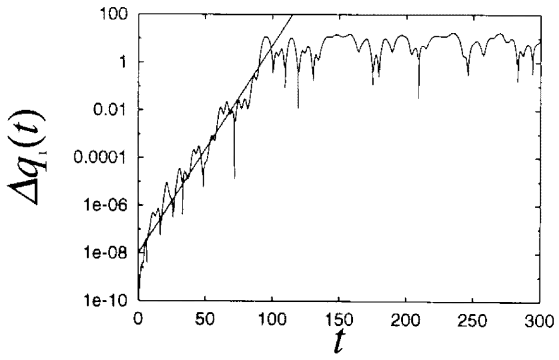

Figure 1.2: Exponential growth of initial difference in a chaotic system. $\Delta q_1(t)$ is the difference between the two orbits shown in Fig.1.1(b).

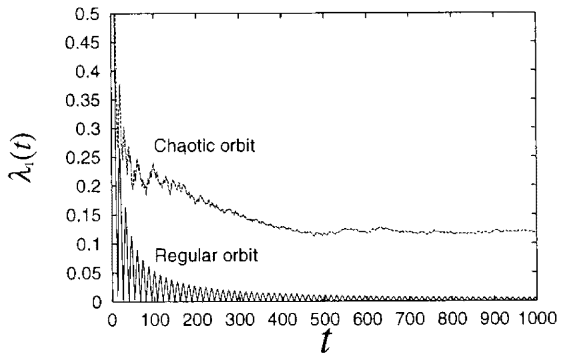

Figure 1.3: Convergence of Lyapunov exponents (A.23) in the regular and the chaotic orbits shown in Fig.1.1.

in Fig.1.1, and the distinction between regular and chaotic motions is clearly found. The power spectrum for the regular motion is a sum of discrete peaks reflecting periodic behaviour of $q_1(t)$. For the chaotic motion power spectrum has broad continuous range, and the motion cannot be understood as just a superposition of regular oscillation.

1.2 Long time tail in chaotic systems

Let us introduce an interesting phenomenon appearing in chaotic systems. In various Hamiltonian systems, for instance, in area preserving mappings [Kar83, CS84], a water cluster [BHSO97] and a ferro-magnetic spin system [Yam97] power spectra take the form called $1/f$ spectrum, that is,

$$S(f) \sim 1/f^{\nu} \quad (0 < \nu < 2). \tag{1.4}$$

Note that the $1/f$ spectrum does not include $\nu = 0$ and $\nu = 2$. The $1/f$ spectrum cannot be yielded by regular orbits because power spectra are superposition of periodic oscillations as seen in Fig.1.4(a).

We rewrite this power spectrum as (auto) correlation function which is defined as

$$C(t) \equiv \lim_{T\to\infty} \frac{1}{2T} \int_{-T}^{T} \Delta X(\tau + t)\Delta X(\tau)\mathrm{d}\tau, \tag{1.5}$$

$$\Delta X(t) \equiv X(t) - \lim_{T\to\infty} \frac{1}{2T} \int_{-T}^{T} X(t), \tag{1.6}$$

where X is an observed quantity. Note that the definition assumes that system is stationary. Wiener-Khinchin theorem states that correlation function is

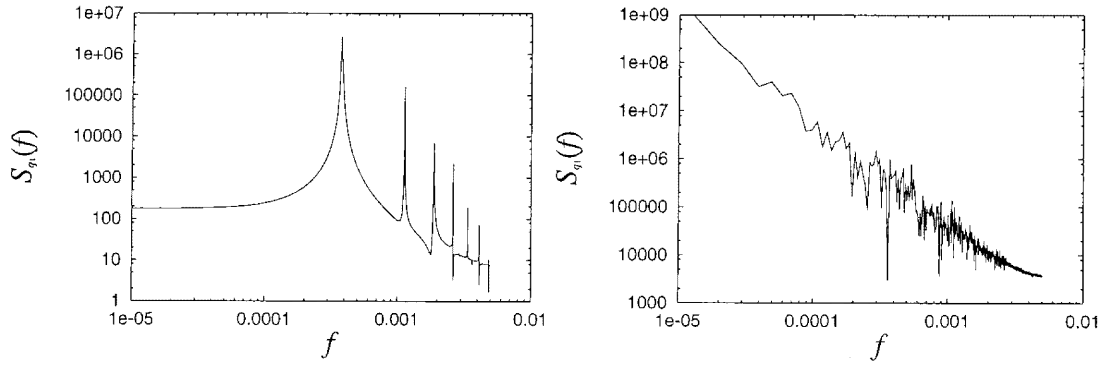

(a) Regular orbit (b) Chaotic orbit

Figure 1.4: Power spectra of $q_1(t)$ for the regular and the chaotic orbits shown in Fig.1.1. (a) For a regular orbit. The power spectrum is a sum of discrete peaks. (b) For a chaotic orbit. The power spectrum has broad continuous range.

equivalent to Fourier transformed power spectrum, and hence

$$\begin{aligned} C(t) &= \int S(f)\mathrm{e}^{ift}df \\ &\sim \int \left(\frac{X}{t}\right)^{-\nu} \mathrm{e}^{iX}\mathrm{d}\left(\frac{X}{t}\right) \\ &= t^{\nu-1}\int X^{-\nu}\mathrm{e}^{iX}\mathrm{d}X. \end{aligned} \tag{1.7}$$

The correlation function $C(t)$ is power type if the integral $I \equiv \int X^{-\nu}\mathrm{e}^{iX}\mathrm{d}X$ converges. When $1 < \nu < 2$ the function $C(t)$ diverges in Eq.(1.7). However, this correlation function is not correct since system breaks the condition being stationary, in other words, the integral I does not converge. Anyway, relaxation of correlation function is power type and slower than exponential type when $1/f$ spectrum appears. This slow relaxation is called long time tail, since the relaxation does not finish for a long period while the exponential relaxation,

$$C(t) \sim \mathrm{e}^{-t/\tau}, \tag{1.8}$$

roughly finishes at the finite time $t = \tau$. In other words, relaxation time τ becomes infinity when $C(t)$ is power type.

At first sight, the long correlation seems inconsistent with that chaotic motion exponentially loses initial information, i.e.

$$|\delta x(t)| \sim |\delta x(0)| \exp(\lambda_1 t), \quad \lambda_1 > 0. \tag{1.9}$$

The inconsistency is caused by confusing local and global properties. Lyapunov exponent λ_1 calculates the average of local instability along an orbit in a long period as described in Appendix A. On the other hand, power spectrum and correlation function includes information of global motion on phase space. Consequently,we must understand global structure of phase space to understand some dynamical properties like the long time tail.

In the next section we review the global structures in the three classes of Hamiltonian systems: integrable, nearly integrable and fully chaotic systems.

1.3 Structures of phase spaces

Hamiltonian systems are usually classified into integrable, nearly integrable and fully chaotic systems, and the classification depends on varieties of orbits. All the orbits are regular in an integrable system, both of regular and chaotic orbits exist in a nearly integrable system, and all the orbits are chaotic in a fully chaotic system. In this section we shortly review the global structures of phase spaces in the three classes with some examples. Details and the definition of integrability are described in Chap.2.

1.3.1 Integrable system

Let us consider the following Hamiltonian system:

$$H(p,q) = \frac{1}{2}p^2 + (1 - \cos q). \tag{1.10}$$

This system represents a simple pendulum, and this is integrable. The phase space of this system is shown in Fig.1.5. The orbits are regular and correspond to librational motion, rotational motion and separatrices. On the phase space the orbits are described as smooth curves $H(p,q) = E$ (constant) because of the energy conservation. Note that long time tail does not appear in integrable systems since all the orbits are regular, and power spectrum for a regular orbit is a sum of discrete peaks.

1.3.2 Nearly integrable system

In nearly integrable systems Hamiltonian is represented as

$$H(p,q) = H_0(p,q) + \epsilon H_1(p,q) + \epsilon^2 H_2(p,q) + \cdots, \tag{1.11}$$

where ϵ is a small parameter, i.e. $|\epsilon| \ll 1$, and all the orbits are regular when $\epsilon = 0$. For these systems perturbative approaches are available. Kolmogorov-Arnold-Moser (KAM) theorem states that regular orbits with non-zero volume survive small perturbation. The regular orbits run on invariant tori, which are called

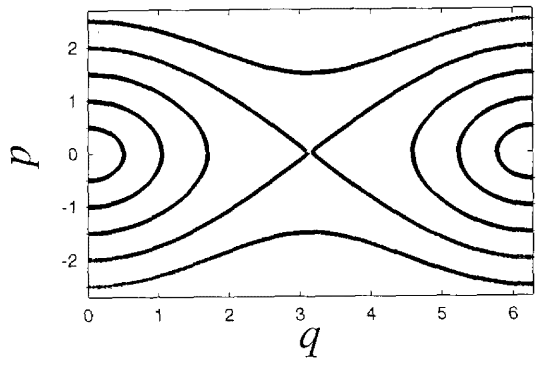

Figure 1.5: The phase space of the system (1.10).

KAM tori. With the aid of Poincaré-Birkhoff theorem, hierarchical structure of phase space is understood which consists of KAM tori and chaotic regions. The KAM tori and hierarchical structure in Hénon-Heiles system is clearly shown in Fig.1.6 which shows a section of a 3-dimensional equal energy surface, where smooth curves, whose topology is the same as circle, are sections of 2-dimensional KAM tori. Hamiltonian of the system is

$$H(p,q) = \frac{1}{2}(p_1^2 + p_2^2) + \frac{1}{2}(q_1^2 + q_2^2) + q_1^2 q_2 + \frac{1}{3}(1 - 2\epsilon)q_2^3, \tag{1.12}$$

and the system is integrable when $\epsilon = 0$ or $\epsilon = -5/2$.

1.3.3 Fully chaotic system

In fully chaotic systems phase spaces have no structure as seen in Fig.1.7. The figure is section of an equal energy surface in the system (1.1) with $\epsilon = 2.0$ and $E = 5.5$, and the figure is produced from only a single orbit. The power spectrum of $q_1(t)$ for the orbit is shown in Fig.1.8, and the power spectrum is $S(f) \sim f^{-2}$. It is a part of Lorentzian ($S(f) \sim 1/(f^2 + a^2)$) since the Lorentzian becomes f^{-2} in a region of large f. According to Wiener-Khinchin theorem, correlation function is exponential when power spectrum is Lorentzian, i.e.

$$C(t) \sim \exp(-t/\tau). \tag{1.13}$$

The motion is therefore regarded as Markovian, and no long time tail appears in this class.

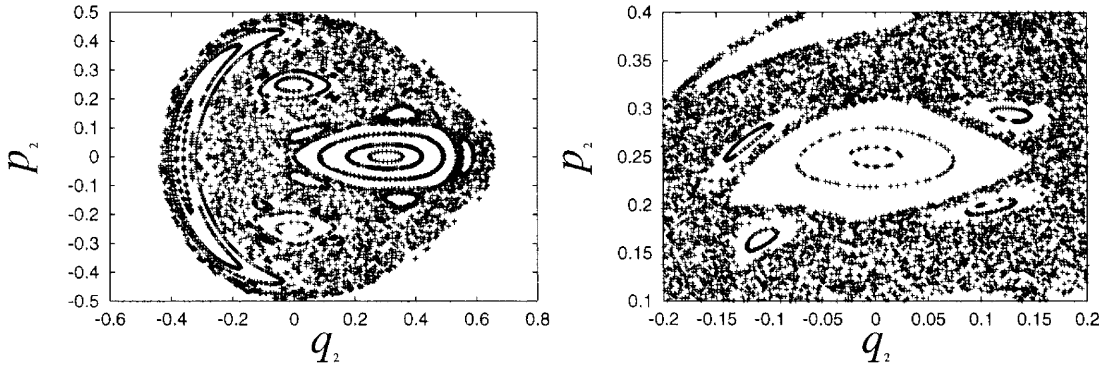

(a) The whole area of the section

(b) A magnified picture of (a)

Figure 1.6: A section of the phase space in Hénon-Heiles system. $E = 0.125$ and $\epsilon = 1$. (b) is a magnified figure of (a), and hierarchical structure is found. Plus symbols (+) are plotted if and only if $q_1 = 0$ and $p_1 > 0$. Circles are sections of 2-dimensional tori.

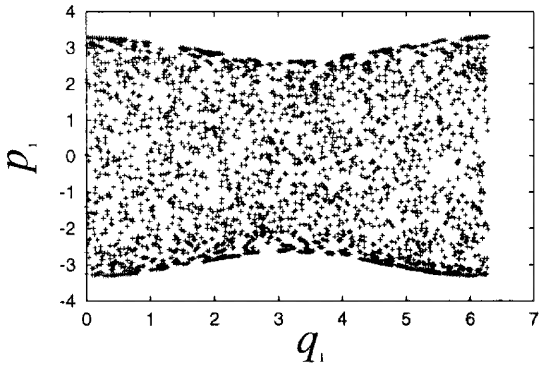

Figure 1.7: A section of the phase space in a fully chaotic system (1.1). $\epsilon = 2.0$. $E = 5.5$. Plus symbols (+) are plotted if and only if $q_2 = 0$ and $p_2 > 0$. No structure is found on the section. This figure is produced from only one initial condition, that is, all the points are on a single orbit.

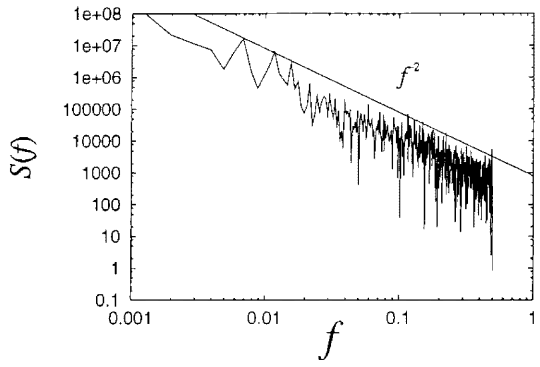

Figure 1.8: The power spectrum of the orbit used in Fig.1.7. It is f^{-2}, which is a part of Lorentzian. The solid line is a guide for eyes.

1.4 The purposes of this thesis

The $1/f$ spectrum cannot be observed in integrable and fully chaotic systems, and hence it have been tried to understand with hierarchical structure consisting of KAM tori in nearly integrable systems. For systems with two degrees of freedom, some studies have connected the hierarchical structure and long time tail like the $1/f$ spectrum. Aizawa introduced a geometrical model with an assumption of exact self-similarity consisting of KAM tori, and this model successfully yields the long time tail. We therefore understand that the long time tail arises from self-similar structure of phase space (often mentioned as "islands around islands" [Mei86]) and motion trapped to KAM tori or their debris Cantori in various scales. Meiss et al. has successfully proposed a similar model [MO86]. Renormalization group approach [Esc85, HI87] which proves similarity between scale transformations in phase space and in time also supports the picture above.

$1/f$ spectra are observed in systems with many degrees of freedom, although they are also observed in systems with 2 degrees of freedom. However, the models [Aiz84, Mei86] are based on that systems have 2 degrees of freedom, and they cannot be directly applied to systems with many (more than 2) degrees of freedom. For such systems Aizawa et al. discuss [AKH$^+$89] the origin of $1/f$ spectra based on Nekhoroshev bound, which is reviewed in Chap.2. However, relation between Nekhoroshev bound and hierarchical structure of phase space is not clear since the former and the latter concern local and global properties on phase space, respectively. Moreover, the assumptions on which the models based do not seem to hold for systems with many degrees of freedom. It is believed that KAM tori rapidly disappear as the system size gets large [Kon94] while the models mainly consider KAM tori.

Now, we conclude that the cause of the long time tail cannot be revealed

in nearly integrable systems when we consider systems with many degrees of freedom, in which we are just interested. Accordingly, we must introduce a new class of chaotic systems which are not nearly integrable but yield long time tail. Systems belonging to the new class have moderate strength of chaos, which is stronger than one in nearly integrable systems but weaker than in fully chaotic systems. We call such systems *moderately chaotic systems.*

The existence of moderately chaotic systems is not obvious, and to show it is one of the purposes of this thesis. The moderately chaotic systems have structure in their phase spaces because motion in them has long correlation. The global structure, which has not been revealed, must give the causes of some interesting dynamical properties like long time tail as it does in nearly integrable systems. The main purposes of this thesis are to reveal the global structure of phase space in the moderately chaotic systems with many degrees of freedom, and to understand long time tail from the structure.

1.5 The construction of this thesis

This thesis is constructed as follows.

We introduce the definition of integrability and show that orbits in integrable systems are essentially periodic in Chap.2. We also review theories for nearly integrable systems with perturbative approaches, and the theories describe properties and hierarchical structure of phase space in details.

In Chap.3 six Hamiltonian systems are introduced and we show that they are moderately chaotic at appropriate values of energy. That they are not nearly integrable is shown by observing no surviving tori, and that not fully chaotic is shown by using a power spectrum and Lyapunov spectra. See Appendix A for details of Lyapunov spectrum.

As an interesting example of phenomena occurring in the moderately chaotic system, second order phase transition is considered in Chap.4. A system having second order phase transition is represented by a Hamiltonian, and it is therefore a Hamiltonian dynamical system temporally evolving with canonical equations of motion. We show slow relaxation of order parameter at the critical point through numerically integrating the equations of motion [Yam96].

In Chaps.5 and 6, we investigate structure of phase space in moderately chaotic systems. We expect that moderately chaotic systems have universal structure in phase spaces as nearly integrable systems universally have hierarchical structure based on KAM tori, and that some quantities must reflect the universal structure. In Chap.5 we show a universal form of Lyapunov spectra [Yam98]. Lyapunov spectrum is a set of Lyapunov exponents, $\{\lambda_i\}$ $(i = 1, 2, \cdots N)$, and it is usually used to calculate instabilities along an orbit. The universality is found only in a range of large i/N, and it appears when the potential function is dominated by quadratic terms rather than higher order terms.

Using the features obtained by analysing Lyapunov spectra, a geometrical model is constructed in Chap.6 to reveal structure of the phase space in the moderately chaotic system [YK98a]. The model is an extension of Aizawa model to high-dimensional systems. The model successfully yields long time tail, and hence it conceptually describes structure of phase space in moderately chaotic systems.

Chapter 7 is devoted to summary and discussions.

Chapter 2

Review of Hamiltonian Dynamical Systems

In this chapter we review theories and tools for Hamiltonian dynamical systems: integrability and non-integrability, resonance, KAM theorem, Poincaré mapping, Poincaré-Birkhoff theorem, Arnold diffusion, Nekhoroshev bound, and Aizawa model.

2.1 Integrable systems

Let us start from the definition of integrability.

Definition 1 (Integrability)

Hamiltonian systems with N degrees of freedom are completely integrable if and only if
1) there are N independent integrals (invariant functions) $\Phi_1, \Phi_2, \cdots, \Phi_N$, and
2) these N integrals are involutive, that is,

$$\{\Phi_i, \Phi_j\} \equiv \sum_{k=1}^{N} \left[\frac{\partial \Phi_i}{\partial q_k} \frac{\partial \Phi_j}{\partial p_k} - \frac{\partial \Phi_i}{\partial p_k} \frac{\partial \Phi_j}{\partial q_k} \right] = 0 \quad (i, j = 1, 2, \cdots, N), \tag{2.1}$$

where $\{\ ,\ \}$ is Poisson bracket.

Here a function $\phi(p, q)$ is invariant if and only if

$$\phi(p(t), q(t)) = \phi(p(0), q(0)), \qquad \text{for } \forall t. \tag{2.2}$$

The definition of integrability is meaningful when non-integrable systems exist, and we show the existence in the next section. Note that systems with one degree of freedom are integrable because Hamiltonian itself is the integral, and the lowest degrees of freedom are 2 to be non-integrable.

Global structure of phase space is revealed by the following theorem [Arn89] in integrable systems.

Theorem 1 (Liouville-Arnold)

Let us consider a level set M_a which is defined as

$$M_a \equiv \{(p,q) \mid \Phi_i(p,q) = a_i \ (i = 1, 2, \cdots, N)\}. \tag{2.3}$$

Energy is constant on this M_a. We assume
(i) the level set M_a is compact and connected, and
(ii) gradient vectors $\{\nabla\Phi_i(p,q)\}$ are linearly independent at each point on M_a.
Then, the topology of M_a is N-dimensional torus T^N, and orbits run on the T^N periodically or quasi-periodically. That is, all the orbits are regular.

Let us roughly understand the Liouville-Arnold theorem and explain what is quasi-periodic motion. We take the action-angle coordinate (J, θ), where J and θ are action and angle vectors respectively, and $J_i = \Phi_i$. In integrable systems motion is determined by N integrals Φ_i's, and Hamiltonian therefore depends only on J_i's, namely $H = H_0(J)$. The subscript 0 represents that the system is integrable. Hamiltonian equations of motion are as follows,

$$\frac{\mathrm{d}J_i}{\mathrm{d}t} = -\frac{\partial H_0}{\partial \theta_i} = 0, \tag{2.4}$$

$$\frac{\mathrm{d}\theta_i}{\mathrm{d}t} = \frac{\partial H_0}{\partial J_i} \equiv \omega_i(J) = \text{constant}, \quad (i = 1, 2, \cdots, N). \tag{2.5}$$

That is, action J_i's are constant and θ_i's evolve linearly with respect to time, i.e. $\theta_i = \omega_i(J)t$. We assumed that invariant manifold M_a is compact, and hence the angle θ must be periodic. We assume the period as 2π, then $\theta_i(t)$ is

$$\theta_i(t) = \omega_i(J)t \pmod{2\pi}. \tag{2.6}$$

Consequently, the N-dimensional hyperplane $(\theta_1, \theta_2, \cdots, \theta_N)$ is topologically equivalent to N-dimensional tori $T^N = (S^1)^N$ (each S^1 corresponds to one of θ_i's).

For simplicity, we set $N = 2$, then equations of motion are

$$\frac{\mathrm{d}\theta_1}{\mathrm{d}t} = \omega_1, \quad \frac{\mathrm{d}\theta_2}{\mathrm{d}t} = \omega_2. \tag{2.7}$$

When the ratio of the two frequencies is rational, that is, $\omega_2/\omega_1 = r/s$ with relatively prime integers r and s, then motion is periodic with period $2\pi s/\omega_1 = 2\pi r/\omega_2$, i.e.

$$\theta_1(t + 2\pi m_1 s/\omega_1) = \theta_1(t), \quad \theta_2(t + 2\pi m_2 r/\omega_2) = \theta_2(t), \tag{2.8}$$

where m_1 and m_2 are arbitrary integers. On the other hand, when the ratio is irrational, an orbit never comes back to the initial point, i.e.

$$\theta_i(t) \neq \theta(0) \quad \text{for } t \neq 0, \tag{2.9}$$

although it densely fills the torus. Examples of periodic and quasi-periodic motions are shown in Fig.2.1.

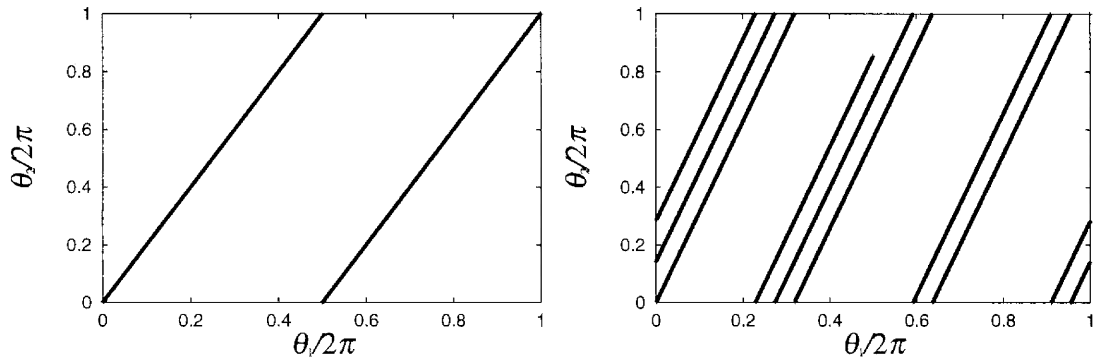

(a) Periodic motion

(b) Quasi-periodic motion

Figure 2.1: Periodic and quasi-periodic motion on a 2-dimensional torus following Eq.(2.7). The lines $\theta_1/2\pi = 0$ and $\theta_2/2\pi = 0$ are identified with the lines $\theta_1/2\pi = 1$ and $\theta_2/2\pi = 1$, respectively. (a) Periodic motion. $\omega_1 = 1$ and $\omega_2 = 2$. (b) Quasi-periodic motion. $\omega_1 = 1$ and $\omega_2 = \pi$. $0 \leq t \leq 2.5\pi$. The quasi-periodic motion densely fills the torus.

2.2 Existence of non-integrable systems

If all the Hamiltonian were integrable, studies of Hamiltonian systems would finish when we write down equations of motion. However, Poincaré showed that perturbed systems are generally non-integrable [Poi92, Poi93].

Theorem 2 (Poincaré)

We consider a perturbed system,

$$H(J,\theta) = H_0(J) + \epsilon H_1(J,\theta) + \epsilon^2 H_2(J,\theta) + \cdots, \tag{2.10}$$

where $H_0(J)$ is integrable part and ϵ is a small parameter, i.e. $|\epsilon| \ll 1$. Let us assume that

(i) $H_1, H_2, \cdots$ are periodic with respect to θ,

(ii) Hessian of H_0 is not degenerate, that is,

$$\det\left(\frac{\partial^2 H_0}{\partial J_i \partial J_j}\right) \neq 0, \tag{2.11}$$

and (iii) H_1 has infinite non-zero Fourier components with respect to θ. Then, the system generally does not have integrals Φ which is analytic with respect to (J,θ,ϵ), independent of H, and expanded as

$$\Phi(J,\theta) = \Phi_0(J) + \epsilon\Phi_1(J,\theta) + \epsilon^2\Phi_2(J,\theta) + \cdots, \tag{2.12}$$

Restricted three bodies system, in which one of the bodies has infinitesimal mass, is an example satisfying the assumptions [Whi].

2.3 Resonance and non-integrability

Let us consider a perturbed Hamiltonian system, Eq.(2.10). Such system is usually solved with regular perturbation. However, the regular perturbation breaks if the following resonance condition is satisfied;

$$k \cdot \omega(J) = \sum_{i=1}^{N} k_i \omega_i(J) = 0, \tag{2.13}$$

where $\omega_i(J) \equiv \partial H/\partial J_i$ and k_i's are arbitrary integers but all the k_i's are not zero simultaneously. Let us see how resonance condition breaks regular perturbation.

The strategy to perturbatively solve the motion is to transform coordinate from (J, θ) into (J', θ') with which Hamiltonian becomes as

$$\begin{aligned} H(J,\theta) &= H_0(J) + \epsilon H_1(J,\theta) && (2.14)\\ &= H_0'(J') + \epsilon^2 H_2(J',\theta'). && (2.15) \end{aligned}$$

If this transformation is successful for infinite times, then we get an integrable Hamiltonian;

$$H(J,\theta) = H_\infty(J_\infty). \tag{2.16}$$

Motion in an integrable Hamiltonian system is easily solved as mentioned in Sec.2.1. The failure of the strategy is shown by giving the concrete expression of the transformed coordinate (J', θ'). We introduce a generator $S(J', \theta)$ of this canonical transformation, i.e.,

$$\begin{aligned} S(J',\theta) &= J' \cdot \theta + \epsilon S_1(J',\theta), && (2.17)\\ J &= J' + \epsilon \frac{\partial S_1}{\partial \theta}, && (2.18)\\ \theta' &= \theta + \epsilon \frac{\partial S_1}{\partial J'}. && (2.19) \end{aligned}$$

Using the generator $S(J', \theta)$, Hamiltonian H is rewritten as

$$\begin{aligned} H &= H_0(J) + \epsilon H_1(J,\theta) && (2.20)\\ &= H_0(J' + \epsilon \frac{\partial S_1}{\partial \theta}) + \epsilon H_1(J' + \epsilon \frac{\partial S_1}{\partial \theta}, \theta) && (2.21)\\ &= H_0(J') + \epsilon \left\{ \frac{\partial S_1}{\partial \theta} \cdot \frac{\partial H_0}{\partial J}(J') + H_1(J',\theta) \right\} + O(\epsilon^2), && (2.22) \end{aligned}$$

and hence the strategy Eq.(2.14) requires that the following equation holds

$$\frac{\partial S_1}{\partial \theta} \cdot \frac{\partial H_0}{\partial J} + H_1(J',\theta) = 0. \tag{2.23}$$

Any functions of θ are periodic with respect to θ since θ is periodic with period 2π, and accordingly, we use Fourier series expansion to get S_1 from Eq.(2.23):

$$H_1(J',\theta) = \sum_{k\neq 0} e^{ik\cdot\theta}\hat{H}_{1,k}(J'), \tag{2.24}$$

$$S_1(J',\theta) = \sum_{k\neq 0} e^{ik\cdot\theta}\hat{S}_{1,k}(J'). \tag{2.25}$$

The summation does not include $k = 0$ because, for instance, $e^{i0\cdot\theta}\hat{H}_{1,0}(J')$ is independent of θ and it can be transferred to $H_0(J')$. Anyway, we substitute these expressions into Eq.(2.23), and get the following equation

$$ik\cdot\omega(J')\hat{S}_{1,k}(J') + \hat{H}_{1,k}(J') = 0, \tag{2.26}$$

that is,

$$\hat{S}_{1,k}(J') = -\frac{\hat{H}_{1,k}(J')}{ik\cdot\omega(J')}, \tag{2.27}$$

where $\omega(J) \equiv \partial H_0/\partial J$ and $k \neq 0$. We therefore obtain the generator $S(J',\theta)$ with the inverse Fourier transformation of $\hat{H}_{1,k}$ as

$$S_1(J',\theta) = -\sum_{k\neq 0} e^{ik\cdot\theta}\frac{\hat{H}_{1,k}(J')}{ik\cdot\omega(J')}, \tag{2.28}$$

$$\hat{H}_{1,k}(J') = \left(\frac{1}{2\pi}\right)^N \int\cdots\int \mathrm{d}\theta e^{-ik\cdot\theta}H_1(J',\theta). \tag{2.29}$$

However, Eq.(2.26) does not give $\hat{S}_{1,k}(J')$ when resonance condition (2.13) is satisfied, and then the strategy breaks.

2.4 KAM theorem

As seen in the previous section, integrability breaks when resonance condition holds. However, not all the orbits become chaotic in a perturbed system. The existence of regular orbits are stated by Kolmogorov-Arnold-Moser (KAM) theorem [Kol54, Arn63, Mos62] when resonance is absent.

Theorem 3 (KAM)

Assume the following three conditions are satisfied:
(1) non-resonance condition

$$\sum_{i=1}^{N} k_i\omega_i(J) \neq 0 \tag{2.30}$$

over some domain of J, where $\omega_i(J) \equiv \partial H_0(J)/\partial J_i$ and the k_i's are the components of the integer vector k;
(2) a smoothness condition on the perturbation $H_1(J,\theta)$, namely H_1 has sufficient number of continuous derivatives;
(3) initial conditions sufficiently far from resonance to satisfy

$$|k \cdot \omega| \geq \gamma |k| - \tau, \tag{2.31}$$

where γ and τ depend on N and ϵ respectively.
Then there exists an invariant torus (J,θ) parameterized by ξ, satisfying the relations

$$J = J_0 + v(\xi,\epsilon), \tag{2.32}$$
$$\theta = \xi + u(\xi,\epsilon). \tag{2.33}$$

Here u and v are periodic in ξ and vanish for $\epsilon = 0$, and $\dot{\xi} = \omega$, the unperturbed frequencies on the torus.

Roughly speaking, KAM theorem states that regular orbits with non-zero volume survive even under a small perturbation. A regular orbit runs on an invariant manifold, torus, and the surviving torus is called KAM torus. For instance, circles in Fig.1.6 are sections of KAM tori. To apply KAM theorem, small parameter ϵ has to satisfy

$$\epsilon < C(N!)^{-\alpha} \tag{2.34}$$

for systems with many degrees of freedom, where C and α are constants independent of N. Consequently, KAM theorem is not practical for systems with many degrees of freedom although it is usually used for conceptual understanding of structure of phase space.

2.5 Poincaré mapping

Poincaré section Σ and Poincaré mapping F are tools to visualize global structure of phase space. The former is a $(2N-2)$-dimensional surface when a system has N degrees of freedom, and the latter is a mapping from Σ to itself and

$$F : (q(t_i), p(t_i)) \mapsto (q(t_{i+1}), p(t_{i+1})), \quad (i = 0, 1, 2, \cdots), \tag{2.35}$$

where we assumed an orbit intersects Σ at t_i (see.Fig.2.2). Figure 1.6 is an example of Poincaré section.

Poincaré mappings are symplectic as Hamiltonian flows are, namely

$$\sum_{i=1}^{N} dp_i(t) \wedge dq_i(t) = \sum_{i=1}^{N} dp_i(0) \wedge dq_i(0), \tag{2.36}$$

and accordingly, $(2N-2)$-dimensional symplectic mappings are regarded as models of Poincaré mappings of systems with N degrees of freedom.

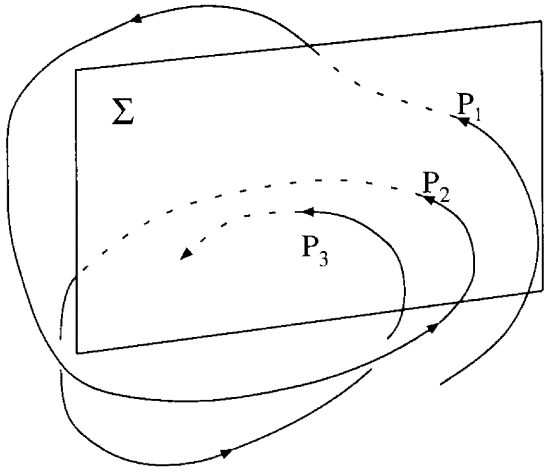

Figure 2.2: Schematic picture of Poincaré mapping F and Poincaré section Σ. The Poincaré mapping F maps P_1 on P_2 and so on. (From master thesis of Y.Hirata [Hir])

2.6 Poincaré-Birkhoff theorem

Hierarchical structure of phase spaces is revealed with the aid of Poincaré-Birkhoff theorem in nearly integrable systems with two degrees of freedom. The hierarchical structure is based on fixed points of Poincaré mapping. We therefore consider fixed points of a Poincaré mappings F with the Poincaré section Σ defined as $\theta_1 = 0$. Note that periodic points with period-m are fixed points of $F^m = F \circ F \circ \cdots \circ F$ ($m-$times), and hence we consider F^m to get generality.

2.6.1 Main theorem

In an integrable system with two degrees of freedom, a Poincaré mapping is easily constructed from Eqs.(2.4) and (2.5) as follows

$$F_0^m : \begin{cases} J' &= J, \\ \theta' &= \theta + 2\pi m \alpha(J) \pmod{2\pi}, \end{cases} \tag{2.37}$$

where $\alpha(J) \equiv \omega_2/\omega_1$, m is an integer, and we used J and θ instead of J_2 and θ_2 respectively. The Poincaré section is the plane (J, θ). Adding a perturbation, the mapping is modified as

$$F_\epsilon^m : \begin{cases} J' &= J + \epsilon f(J,\theta), \\ \theta' &= \theta + 2\pi\alpha(J)m + \epsilon g(J,\theta) \pmod{2\pi}, \end{cases} \tag{2.38}$$

where f and g are periodic in θ. If $\alpha(J_0)$ is a rational number, namely $\alpha(J_0) = r/s$ and both r and s are integers, all the points on the curve $J = J_0$ are periodic

points of F_0^m with period-s, namely fixed points of F_0^{ms}. Poincaré-Birkhoff theorem guarantees existence of periodic points after the perturbation.

Theorem 4 (Poincaré-Birkhoff)

Assume that frequencies ω_1 and ω_2 satisfy non-resonance condition (see Eq.(2.30)), in other words, $\alpha(J)$ is not rational. Then, for some integers k, there exist ks hyperbolic fixed points and ks elliptic ones of F_ϵ^{ms}.

Here fixed points of a symplectic mapping are hyperbolic, elliptic or parabolic whose eigen values of the linearized mapping are $(r, 1/r)$ $(\exp(i\nu), \exp(-i\nu))$ or $(1, 1)$, respectively (cf. Fig.6.1). This theorem is easy to prove and the proof is shown using Fig.2.3 as follows.

Let us define a curve C_0 as

$$C_0 \equiv \{(J, \theta) | J = J_0, \text{and } \alpha(J_0) = r/s\} \tag{2.39}$$

in the unperturbed system. We can prove $\alpha'(J) = \mathrm{d}\alpha(J)/\mathrm{d}J \neq 0$ from the non-resonance condition (although no proof is given here), and we hence assume $\alpha'(J) > 0$ without loss of generality. Since $\alpha'(J) > 0$, the following relations are satisfied,

$$\begin{cases} J < J_0 & \rightarrow \quad \theta' < \theta \\ J > J_0 & \rightarrow \quad \theta' > \theta, \end{cases} \tag{2.40}$$

and the relations are assumed to hold in the perturbed system for ϵ being small.

We introduce a smooth curve C_ϵ as

$$C_\epsilon \equiv \{(J, \theta) | \theta' = \theta\} \tag{2.41}$$

near the curve C_0 in the perturbed system. The curve C_ϵ is well defined since C_ϵ intersects the line θ =constant at the only one point owing to $\alpha'(J) > 0$. Points on the curve C_ϵ are radially mapped, and two curves C_ϵ and $F_\epsilon^{ms}(C_\epsilon)$ must enclose an equal area due to the symplectic property of F_ϵ^{ms}. This is only possible if the two curves cross each other an even number of times, and the crossing points are fixed points of F_ϵ^{ms}. Moreover, the fixed points alternate between hyperbolic and elliptic types.

2.6.2 Hierarchical structure

At the centre of Fig.2.3 an elliptic fixed point exists, and Poincaré-Birkhoff theorem guarantees existence of even number of fixed points around the elliptic fixed point. Flows around half the fixed points which are elliptic are similar to the one around the fixed point at the centre except for their scales, and Poincaré-Birkhoff theorem is available around the smaller elliptic fixed points in the same manner. This story is hierarchically adopted, and consequently, the structure is hierarchical in the phase space (cf Fig.1.6).

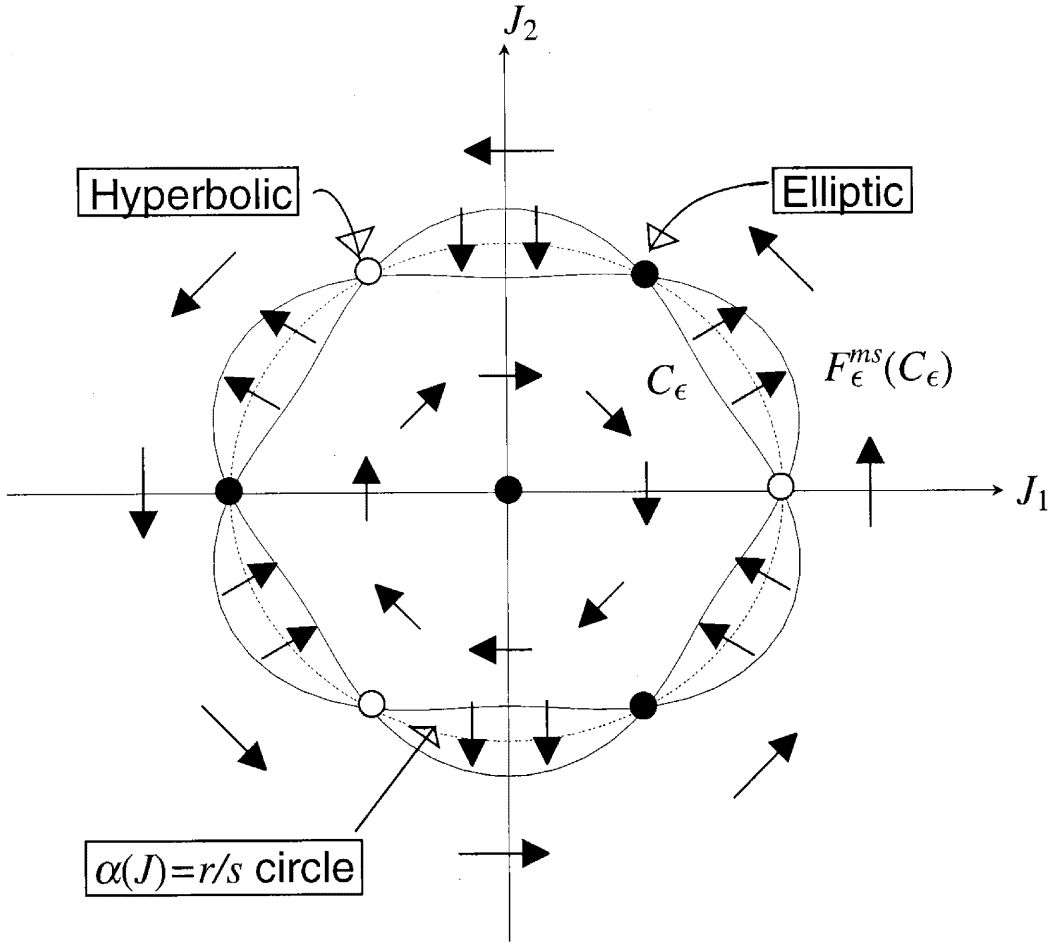

Figure 2.3: Illustrating the Poincaré-Birkhoff theorem that some fixed points are preserved in a small perturbation. The intersections of two solid curves are the preserved fixed points.

2.7 Arnold diffusion

In nearly integrable systems with 2 degrees of freedom, a 3-dimensional energy surface is divided by 2-dimensional KAM tori since KAM tori are invariant surfaces and orbits cannot go across them. Consequently, motion in a chaotic region cannot visit other chaotic regions.

Does this enclosure generally happen even if systems have N (> 2) degrees of freedom ? The $(2N-1)$-dimensional energy surface cannot be divided by N-dimensional KAM tori since codimension of the KAM tori is $N-1$ (> 1). Chaotic region is hence connected, and an orbit may visits the whole chaotic region. This global motion travels in web of resonant layers which are neighborhoods of resonant surfaces satisfying Eq.(2.13), and the motion is slow and behaves like diffusion. The web of resonant layers and the diffusive motion are called Arnold web and Arnold diffusion. The slowness is mathematically analysed by Nekhoroshev as shown in the next section.

2.8 Nekhoroshev bound

The action variable J is constant in integrable systems but not constant in nearly integrable systems, and an orbit hence departs from a torus $J = J_0$. Nekhoroshev gives an upper bound for time derivative of J as follows [Nek77] .

Theorem 5 (Nekhoroshev)

Let Hamiltonian be the same as Eq.(2.10), and we assume that $H_0(J)$ has lowest order terms given by a quadratic form $H_0 = J_0^2/2 + \cdots$, then

$$|\dot{J}| \leq |\omega||J|\epsilon^{1+q}\exp(-1/\epsilon^q), \tag{2.42}$$

with

$$q(N) = \frac{2}{3N^2 - N + 8}. \tag{2.43}$$

This estimate of the upper bound is called Nekhoroshev bound.

Recently, improved $q(N)$ is reported in [LN92] as

$$q(N) = \frac{1}{2N}. \tag{2.44}$$

Anyway, the upper bound of $|\dot{J}|$ is zero for $\epsilon = 0$ and increases with ϵ and N, and hence an orbit tends to apart from a torus $J = J_0$ in a short period in perturbed systems with many degrees of freedom.

2.9 Aizawa model

Hierarchical structure in the 2-dimensional Poincaré mapping can be understood in a unified manner with the model by Aizawa [Aiz84, AKH+89]. The model describes an abstract dynamics rather than a particular dynamics, and it assumes complete self-similarity on the phase space.

The self-similarity consists of KAM tori and chaotic regions, and a KAM torus is surrounded by smaller KAM tori which correspond to higher order resonances. We assign a "level-l" to each KAM torus by that if a KAM torus A is surrounded by KAM tori B_i $(i = 1, 2, \cdots)$ then level-(B_i) = level-(A) +1. There exist infinitely deep levels. Motion around a KAM torus is sticky as shown by Nekhoroshev.

Basic assumptions of the model are as follows.

- The number of KAM tori which surround an KAM torus is independent of the level-l. Let us denote the number of the surrounding KAM tori as ρ.
- The sticky zones around the KAM tori in successive levels have constant ratio. We denote the ratio as

$$\frac{\text{Area}(T_l)}{\text{Area}(T_{l+1})} = b \ (= \text{constant}), \tag{2.45}$$

  where T_l is a KAM torus in level-l.
- Temporal evolution in the level-l chaotic seas is the same as the level-$(l+1)$ chaotic seas whose time scale is multiplied by b.

The total sticky zones around KAM tori is

$$\sum_{l=0}^{\infty} a_0 \left(\frac{\rho}{b}\right)^l = a_0 \frac{1}{1 - \frac{\rho}{b}} \tag{2.46}$$

thus it is assumed $\rho < b$. These assumptions yield the following results.

- Residence time distribution $R(t)$ in the level-l chaotic layer is

$$R(t) \sim t^{-D}, \quad \text{where } D \equiv \frac{\log b}{\log \rho}. \tag{2.47}$$

  The average residence time hence diverges $< t >= \infty$ when $D < 2$.
- Power spectrum $S(f)$ of an angle with respect to the central elliptic fixed point is power law type,

$$S(f) \sim f^{-(3-D)} \quad (f \ll 1). \tag{2.48}$$

- The distribution of areas of KAM tori obeys "fat fractal" and the exponent β is

$$\beta = 2(1 - D'), \quad D' \equiv 1/D(< 1). \tag{2.49}$$

- Distribution of Lyapunov exponent is

$$P(\lambda) \sim \lambda^{-(2-D)}. \tag{2.50}$$

The model therefore catches the essential features of power law behaviours in 2-dimensional Poincaré mappings.

The model is thus useful, but it is available only in the 2-dimensional mappings since it assumes that KAM tori enclose areas of phase space (cf. Sec.2.7). We must extend the model when we consider higher dimensional Poincaré mappings. We construct an extended model in Chap.6.

Chapter 3

Moderately Chaotic Systems

In this chapter we show existence of moderately chaotic systems which are neither nearly integrable nor fully chaotic. At first, we introduce six Hamiltonian systems in Sec.3.1. That the systems are not nearly integrable is shown in Sec.3.2 where we use that nearly integrability is characterized by that many KAM tori with non-zero volume survive. Two ways are introduced to confirm that systems are not fully chaotic. In Sec.3.3 power spectrum is used and in Sec.3.4 we use that fully chaotic systems give straight behaviour of Lyapunov spectra.

3.1 Models

We introduce the following six Hamiltonian systems. One of them is a globally coupled system of XY spin, and the others consist of nonlinear oscillators each of which is on a lattice point of the 3-dimensional simple cubic lattice with nearest neighbour interactions and periodic boundary condition. All the Hamiltonians consist of kinetic and potential terms,

$$H(q,p) = \frac{1}{2}\sum_{j=1}^{N} p_j^2 + U(q), \tag{3.1}$$

where N is the number of degrees of freedom.

The first is a Globally Coupled (GC) system ,

$$U_{GC}(q) = \frac{1}{N}\sum_{i<j}[1-\cos(q_i - q_j)], \qquad q_j \in [0, 2\pi), \tag{3.2}$$

The others are on the 3-dimensional simple cubic lattice. One of them is called XY model and expressed as follows

$$U_{XY}(q) = \sum_{<ij>}[1-\cos(q_i - q_j)], \qquad q_j \in [0, 2\pi), \tag{3.3}$$

where the summation $\sum_{<ij>}$ takes over all the pairs of nearest neighbour lattice points i and j.

The following three systems are expressed as

$$U(q) = \sum_{<ij>} \frac{1}{2}(q_i - q_j)^2 + \sum_{j=1}^{N} V(q_j), \tag{3.4}$$

and they are distinguished by their potential functions $V(q)$. In Double Well (DW) model

$$V_{DW}(q) = -\frac{1}{2}q^2 + \frac{1}{4}q^4, \tag{3.5}$$

in Single Well (SW) model

$$V_{SW}(q) = \frac{1}{2}q^2 + \frac{1}{4}q^4, \tag{3.6}$$

and in Lorentzian (LO) model

$$V_{LO}(q) = \frac{q^2}{1+q^2}. \tag{3.7}$$

The last one has interactions of FPU-β type (3DFPU)

$$U_{3DFPU} = \sum_{<ij>} \left[\frac{k}{2}(q_i - q_j)^2 + \frac{1}{4}(q_i - q_j)^4\right], \tag{3.8}$$

where the proper FPU-β model is on the 1-dimensional chain.

Numerical integrations of Hamiltonian equations of motion,

$$\frac{\mathrm{d}q_j}{\mathrm{d}t} = \frac{\partial H(q,p)}{\partial p_j}, \quad \frac{\mathrm{d}p_j}{\mathrm{d}t} = -\frac{\partial H(q,p)}{\partial q_j}, \quad (j = 1, 2, \cdots, N), \tag{3.9}$$

are performed with fourth order symplectic integrator [Yos93] with the fixed time slice $\Delta t = 0.01$. Accuracy of total energy is $\Delta E/E \sim O((\Delta t)^4)$ where ΔE and E are error and an initial value of total energy, respectively.

3.2 That the systems are not nearly integrable

In a nearly integrable system KAM tori with non-zero volume survive, and local Lyapunov exponent indicates existence of KAM tori. The definition of local Lyapunov exponent is as follows.

$$\lambda_1^{\mathrm{loc}}(n) = \frac{1}{\tau}\int_{n\tau}^{(n+1)\tau} \lambda_1(t)dt, \tag{3.10}$$

$$\lambda_1(t) = \frac{\mathrm{d}}{\mathrm{d}t} \log |X(t)|, \tag{3.11}$$

where $X(t) = (\delta p, \delta q)$ is a $2N$-dimensional tangent vector following linearized Hamiltonian equations of motion,

$$\frac{\mathrm{d}}{\mathrm{d}t} \begin{pmatrix} \delta p \\ \delta q \end{pmatrix} = \begin{pmatrix} 0 & -A(q) \\ 1_N & 0 \end{pmatrix} \begin{pmatrix} \delta p \\ \delta q \end{pmatrix}. \tag{3.12}$$

The sign 1_N is the unit matrix of $N \times N$, and (i, j) element of the matrix $A(q)$ is

$$A_{ij}(q) = \frac{\partial^2 U(q)}{\partial q_i \partial q_j}. \tag{3.13}$$

The local Lyapunov exponent indicates instability along an orbit in a short period τ, and it takes near zero around KAM tori while it takes large value in chaotic region. In nearly integrable systems motion is stagnant around KAM tori and intermittently goes to chaotic region, and local Lyapunov exponent shows intermittency accordingly. An example of intermittency of local Lyapunov exponent is shown in Fig.3.1.

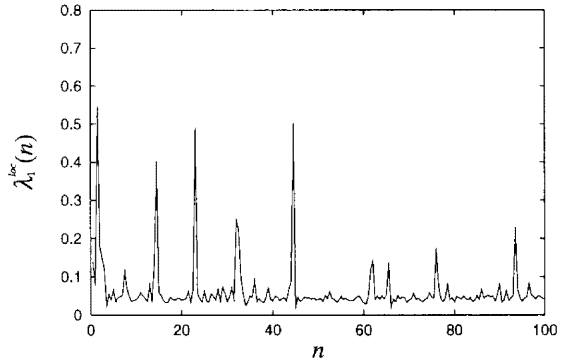

Figure 3.1: An example of intermittency of local Lyapunov exponent $\lambda_1^{\mathrm{loc}}(n)$ in XY model. $E/N = 1.0$ and $N = 10^3$. $\tau = 10$. The state point in phase space is near KAM tori and the chaotic region when $\lambda_1^{\mathrm{loc}}(n)$ takes the lower value and peaks, respectively. This system is nearly integrable since enough KAM tori survive.

Now, local Lyapunov exponents $\lambda_1^{\mathrm{loc}}(n)$ for the six systems are shown in Fig.3.2. Comparing with Fig.3.1, no intermittency is found, and hence the systems effectively have no KAM tori in their phase space. That is, they are not nearly integrable at least for values of energy used here.

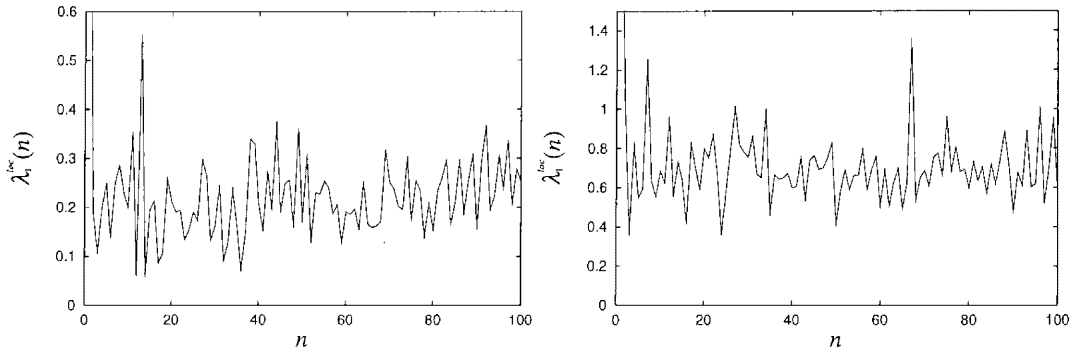

(a) GC

(b) XY

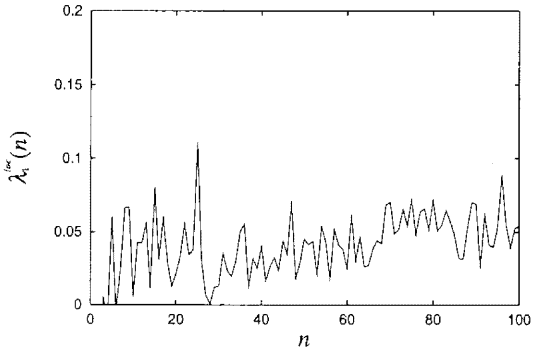

(c) DW

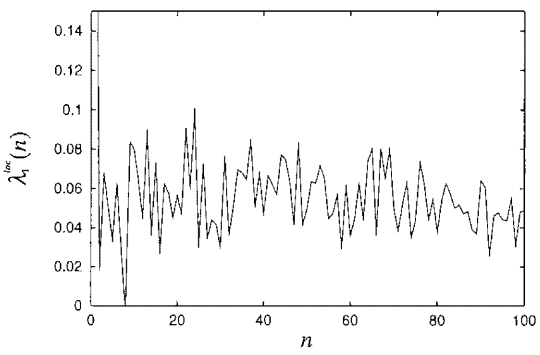

(d) SW

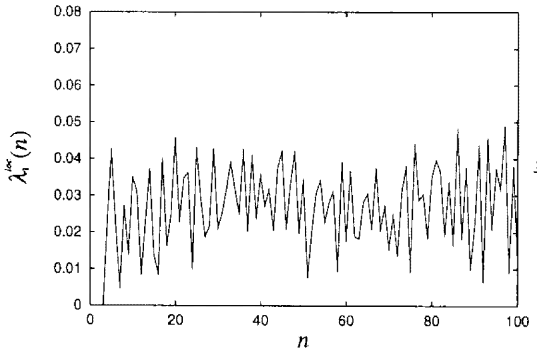

(e) LO

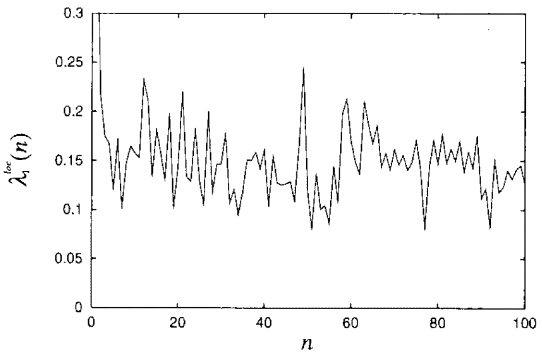

(f) 3DFPU

Figure 3.2: Time series of local Lyapunov exponent for the six systems. The bottom of the figures is zero and no intermittency is found, and hence the systems are not nearly integrable. $N = 64 = (4^3)$. (a) GC: $E/N = 0.75$. (b) XY: $E/N = 3.0$. (c) DW: $E/N = 2.2$. (d) SW: $E/N = 3.0$. (d) LO: $E/N = 2.0$. (e) 3DFPU: $E/N = 1.0$, $k = 1.0$.

3.3 That the systems are not fully chaotic I (power spectra)

Observation of power spectrum is the first way to check whether a system is fully chaotic or not. In fully chaotic system motion is regarded as Markovian (cf. Sec.1.3.3) and correlation of a certain quantity is δ- or exponential function. Power spectrum $S(f)$ of the quantity is hence white ($S(f) \sim$ constant) or Lorentzian ($S(f) \sim 1/(f^2+a^2)$, where a is real). Consequently, the system is not fully chaotic if a power spectrum is neither white nor Lorentzian. We adopt this check to GC model. In Fig.3.3 we show an average of power spectra of momenta $S_p(f)$ which is defined as

$$S_p(f) = \frac{1}{N_0} \sum_{j=1}^{N_0} S_{p_j}(f), \tag{3.14}$$

where $S_{p_j}(f)$ is power spectrum of momentum $p_j(t)$ and N_0 is the number of samples. We set $E/N = 0.75$, $N = 80$ and $N_0 = 40$. The spectrum $S_p(f)$ has power type, namely $S_p(f) \sim f^{-1.2}$, and accordingly, the system is not fully chaotic.

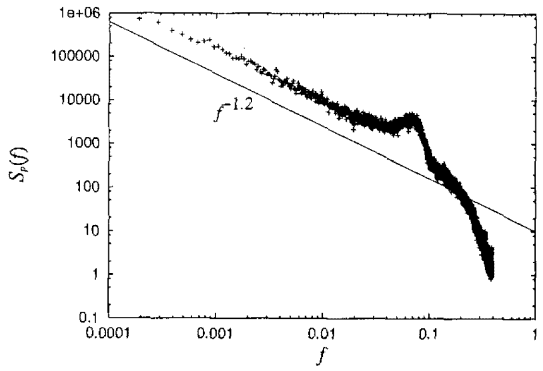

Figure 3.3: An average of power spectra of momenta in GC model. The spectrum $S_p(f)$ is neither white nor Lorentzian, and $S_p(f) \sim f^{-1.2}$. The solid line is a guide for eyes.

3.4 That the systems are not fully chaotic II (Lyapunov spectra)

Using Lyapunov spectrum is the second way of the check. A universal form of Lyapunov spectra $L(i/N) = \lambda_i$ is reported in Hamiltonian systems which are 1-

dimensional chains consisting of nonlinear oscillators [LPR87]. This universality gives the straight form of Lyapunov spectra, namely $L(i/N) = a + b \cdot i/N$, and the straight form is also obtained with random matrices [LPR87, EW88]. Consequently, systems having straight Lyapunov spectra are regarded as fully chaotic ones which have not structure in their phase spaces. In this section we show that the left five systems (XY, DW, SW, DW and 3DFPU) have non-straight Lyapunov spectra, and accordingly, they are not fully chaotic. Let us start to confirm that random matrices give straight Lyapunov spectra even if systems are on the 3-dimensional simple cubic lattice.

3.4.1 Lyapunov spectra of random matrices

Lyapunov spectrum is calculated from linearized Hamiltonian equations of motion, Eq.(3.12), and temporal evolution of the matrix $A(q)$ is determined by temporal evolution of $q_j(t)$'s. When we calculate Lyapunov spectra with random matrices we assume that $q_j(t)$'s are independent random variables with δ- or exponential correlations, namely

$$C_{ij}(t) \propto \delta_{ij}\delta(t) \quad \text{or} \quad \delta_{ij}e^{-\alpha t}, \tag{3.15}$$

respectively. $C_{ij}(t)$ is the correlation function between $q_i(t)$ and $q_j(t)$, and it is defined as

$$C_{ij}(t) = \overline{\Delta q_i(t)\Delta q_j(0)} = \lim_{T\to\infty} \frac{1}{2T}\int_{-T}^{T} dt' \Delta q_i(t+t')\Delta q_j(t'), \tag{3.16}$$

and

$$\Delta q_j(t) = q_j(t) - \lim_{T\to\infty} \frac{1}{2T}\int_{-T}^{T} dt q_j(t). \tag{3.17}$$

We show Lyapunov spectra in Fig.3.4 which are calculated by using random matrices with the δ-correlation, and the Lyapunov spectra are straight as they are in 1-dimensional chains. We took random variables from the uniform distribution, and ranges of $q_j(t)$'s are $[-\pi, \pi)$ for XY model, and $[-3, 3]$ for DW and SW models.

Next we change δ-correlation into exponential, and we set $\alpha = 0.4, 0.6, 0.8$ and 1.0 where α is the reciprocal number of correlation time of $q_j(t)$ (see Eq.(3.15)). Figure 3.5 shows Lyapunov spectra obtained by using random matrices with exponential correlation, and the Lyapunov spectra are also straight in the region of $0.2 \lesssim i/N \leq 1$. Consequently, we suppose that finite correlation time does not affect the straightness of Lyapunov spectra.

Random matrices with δ- or exponential correlation yield straight Lyapunov spectra, and fully chaotic systems hence give the straightness even in the 3-dimensional simple cubic lattice. This result is used later to distinguish our systems evolved by Hamiltonian equations of motion from fully chaotic ones.

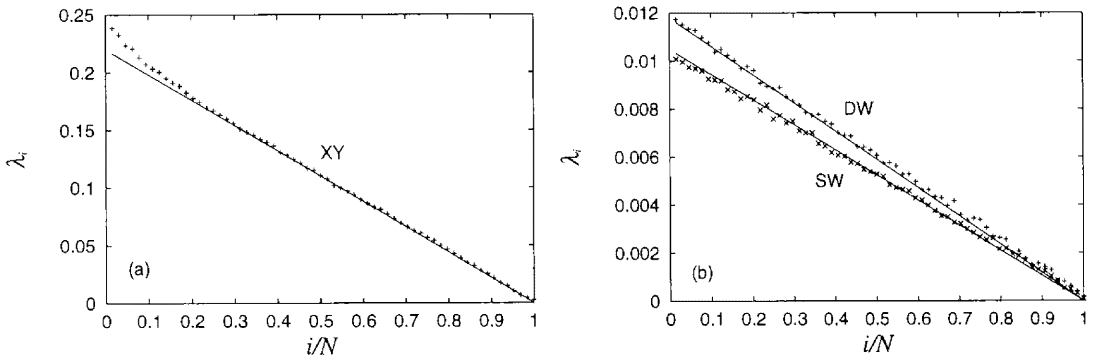

(a) XY (b) DW and SW

Figure 3.4: Lyapunov spectra yielded by using random matrices with δ-correlation for XY, DW and SW models. (a) XY model. (b) DW (+) and SW ($\times$) models. They are straight even in systems on 3-dimensional lattices as they are in 1-dimensional chains. Random variables follow uniform distributions. The straight solid lines are guides for eyes.

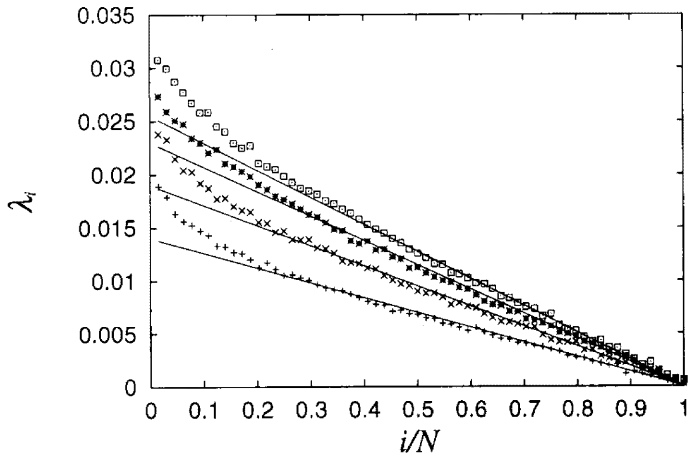

Figure 3.5: Lyapunov spectra yielded by using random matrices with exponential correlation for DW. α, the reciprocal number of correlation time, is $0.4, 0.6, 0.8$ and 1.0 from lower to upper. Spectra show straight behaviour as figure 3.4 in the region of $0.2 \lesssim i/N \leq 1$. The straight solid lines are guides for eyes.

3.4.2 Lyapunov spectra with dynamics

Lyapunov spectra calculated with dynamics are shown in Fig.3.6. The value of energy is the same used in Fig.3.2 for each system. The five Lyapunov spectra are not straight, and the systems are not fully chaotic accordingly. Consequently, the five systems are moderately chaotic.

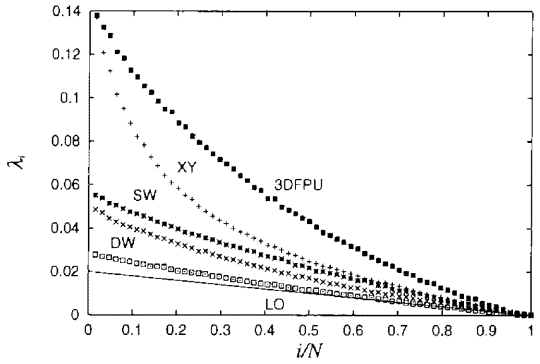

Figure 3.6: Lyapunov spectra calculated with dynamics for the left five systems: XY, DW, SW, LO and 3DFPU. The five Lyapunov spectra are not straight, and the systems are not fully chaotic accordingly. The vertical scale of the Lyapunov spectrum for XY is reduced to 20%. The straight solid line is a guide for eyes.

3.5 Short summary

In this chapter we introduced six Hamiltonian systems and checked whether they are moderately chaotic. A moderately chaotic system is poor in KAM tori but not fully chaotic. Absence of KAM tori was checked by that local Lyapunov exponents do not show intermittency. A power spectrum and Lyapunov spectra were used to confirm that the systems are not fully chaotic. From the two results, we showed that the systems are moderately chaotic although the existence of moderately chaotic systems was not obvious.

Chapter 4

Second Order Phase Transition

We showed existence of moderately chaotic system in the previous chapter, and we study dynamical properties of moderately chaotic system in this and the next chapters. In this chapter we show slow relaxation of order parameter at the critical point of second order phase transition [Yam96] as an interesting phenomenon occurring in the moderately chaotic system.

4.1 Slow relaxation

Slow relaxation at the critical point is phenomenologically discussed by van Hove theory. The temporal evolution of time dependent order parameter $M(t)$ is determined by gradient of Landau's free energy $F(M)$, that is,

$$\frac{dM(t)}{dt} \propto -\frac{\partial F(M)}{\partial M}, \tag{4.1}$$

$$F(M) = a(T)M^2 + b(T)M^4. \tag{4.2}$$

From the solution of Eq.(4.1), we obtain the following temporal evolution of $M(t)$ near the critical temperature T_c

$$M(t) \sim \begin{cases} \exp(-t/\tau(T)) & (\text{when } T \gtrless T_c) \\ t^{-1/2} & (\text{when } T = T_c) \end{cases}, \tag{4.3}$$

where $\tau(T)$ is called relaxation time which depends on temperature T and diverges at T_c.

The GC model (3.2), which is introduced in the previous chapter, has second order phase transition in the meaning of statistical mechanics, and the critical energy E_c is $E_c/N = 0.75$ [AR95] where N is the number of degrees of freedom. According to Figs.3.2(a) and 3.3, the system is moderately chaotic at the critical energy. We show slow relaxation of order parameter $M(t)$ by numerically integrating equations of motion without any assumptions while the phenomenological theory requires some non-trivial assumptions.

4.2 The definition of order parameter

An order parameter M of GC model is defined as follows,

$$M = \lim_{L\to\infty} \frac{1}{L} \int_0^L dt M(t) \tag{4.4}$$

and

$$M(t) = ||\vec{M}(t)||, \quad \vec{M}(t) = \left(\frac{1}{N} \sum_{i=1}^{N} \cos q_i(t), \ \frac{1}{N} \sum_{i=1}^{N} \sin q_i(t) \right), \tag{4.5}$$

where t and $||\vec{M}(t)||$ represent time and absolute value of $\vec{M}(t)$, respectively. Each particle of GC model is on the unit circle, and $N\vec{M}(t)$ is the summation of all the position vectors. When all the particles distribute uniformly on the unit circle at each time, then $M = 0$. On the other hand, when particles form the cluster, which is the only one in this system [Ina93], then $0 < M(\leq 1)$. For this system, Antoni and Ruffo showed that energy dependence of the order parameter in dynamics agrees with one in statistical mechanics [AR95] (see also Fig.4.1).

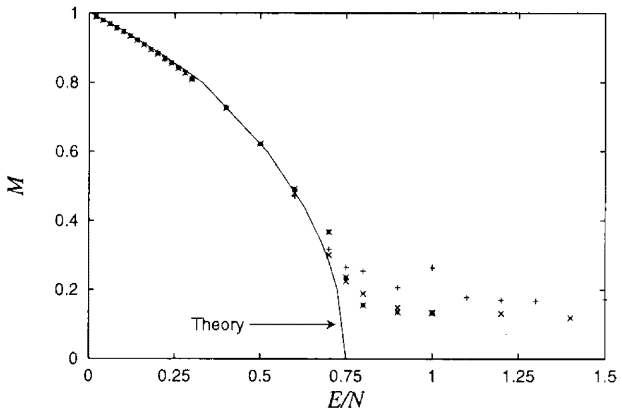

Figure 4.1: Energy dependence of order parameter. The solid curve is obtained by using statistical mechanics. $(+) : N = 40, (\times) : N = 80, (*) : N = 200$. Distinction between the theory and numerical experiments are due to finiteness of degrees of freedom, and numerical experiments tend to agree with the theory as N increases.

4.3 Critical phenomenon in dynamics

We show slow relaxation of order parameter at the critical point. To suppress fluctuation we define local order parameter $M_\tau(n)$ which is defined as

$$M_\tau(n) = \frac{1}{\tau}\int_{(n-1)\tau}^{n\tau} dtM(t), \tag{4.6}$$

and all the relaxation processes are observed through this quantity. At first, slow relaxation of power type is shown, and then we study N dependence of the slow relaxation. To observe relaxation of the order parameter, we initially take small values for q_i's and set $M \sim 1$, where all the q_i's and p_i's follow Gaussian distribution. Scales of p_i's are defined from total energy.

4.3.1 Slow relaxation at critical energy

We report time series of local order parameter $M_\tau(n)$ for $E/N = 0.5, 0.75(= E_c/N)$ and 1 in Fig.4.2. Figure 4.3 shows the following quantity as a function of time t

$$M(t;t_0) = \frac{1}{t-t_0}\int_{t_0}^{t} dtM(t). \tag{4.7}$$

This quantity is time average of $M(t)$ from t_0 to t. We set $t_0 = 1000$ since slow relaxation of $M_\tau(n)$ starts around the t_0. From Fig.4.3, we confirm that the relaxation is power type, namely

$$M(t) \sim t^{-\beta}, \qquad \beta \sim 0.18, \tag{4.8}$$

where the time series $M(t)$ is the same as one used in Fig.4.2(b).

4.3.2 N dependence of the slow relaxation

Second order phase transition occurs in the thermodynamic limit ($N \to \infty$), and hence we must check whether the slow relaxation appears even if we change degrees of freedom N. When $N = 40$, slow relaxation is observed in Fig.4.4 as $N = 80$.

Figure 4.4(b) $M(t;t_0)$ against t, where we set $t_0 = 500$. The $M(t;t_0)$ is power type again, that is, $M(t;t_0) \sim t^{-\beta}$ and $\beta \sim 0.25$. Since we find slow relaxation for different N, we guess slow relaxation appears in the thermodynamic limit. Then relaxation time will be infinity.

4.4 Short summary

We showed slow relaxation of order parameter at the critical point of second order phase transition. The slow relaxation is supposed to appear in the thermodynamic limit although the appearance depends on initial condition [Yam96].

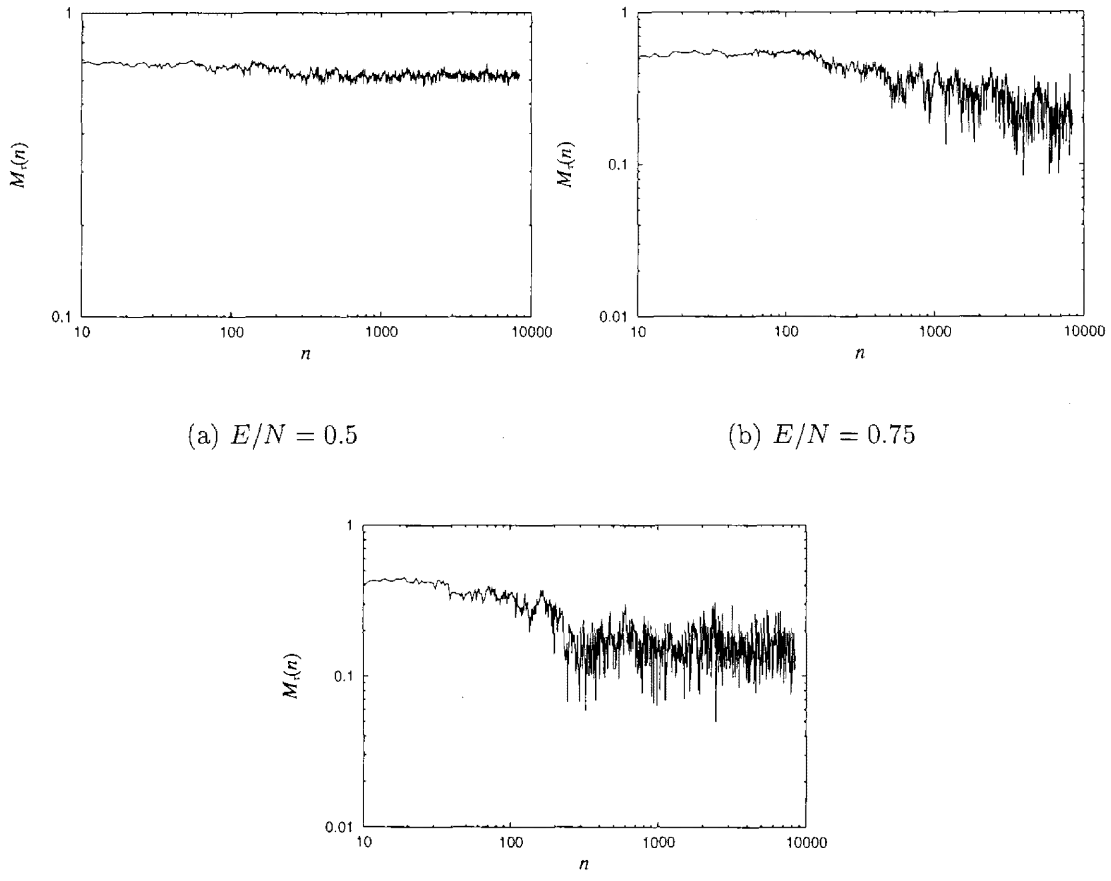

(a) $E/N = 0.5$

(b) $E/N = 0.75$

(c) $E/N = 1.0$

Figure 4.2: Temporal evolutions of local order parameter $M_\tau(n)$. $N = 80$. $\tau = 10$. (a) $E/N = 0.5$. (b) $E/N = 0.75 = E_c/N$. (c) $E/N = 1.0$. The temporal evolution is power type from $t = 1000$ at the critical energy.

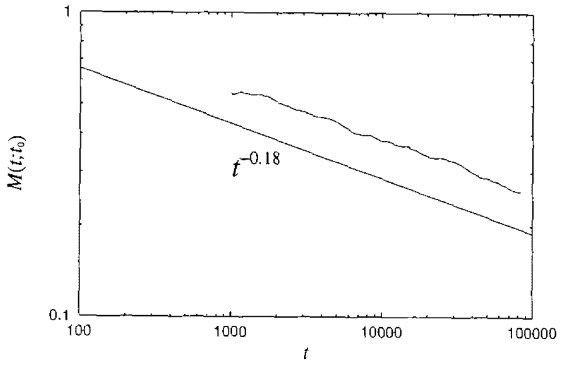

Figure 4.3: Temporal evolution of $M(t;t_0)$. $t_0 = 1000$. Relaxation of power type is clearly found.

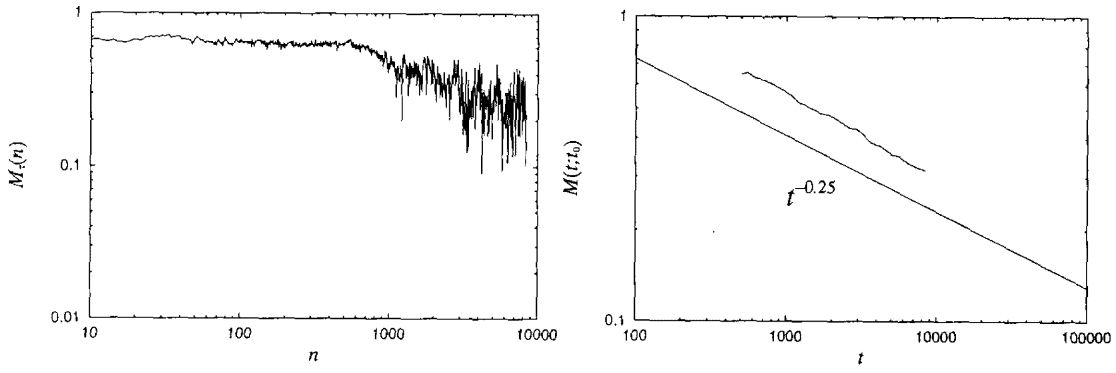

(a) $N = 40$ (b)

Figure 4.4:

As far as I know, this is the first time to show the slow relaxation from direct calculations of Hamiltonian equations of motion. The equations give temporal evolutions of the system without any assumptions even at the critical point, and hence they are useful to study dynamical properties of critical phenomena as shown in this chapter.

Chapter 5

Universality of Lyapunov spectra

Lyapunov spectrum is usually used to study instability along a sample orbit. Moreover, it is useful to study structure of phase spaces both in dissipative [IM86, NK95] and Hamiltonian [MB93, YO87] systems with many degrees of freedom, since it includes information on the whole degrees of freedom. Although Lyapunov spectrum in a system reveals dynamical properties of the system, we are interested further in properties which are not affected by details of systems. To detect such properties a useful approach is to find the universal form of Lyapunov spectra which is obtained in all the systems and whose cause indicates such properties. For instance, straight behaviour of Lyapunov spectra $L(i/N) = \lambda_i$ is universal in fully chaotic systems as mentioned in Sec.3.4.

In this chapter, we show new universality of Lyapunov spectra appearing in moderately chaotic systems, and investigate condition with which the universality appears. Here we define the word "universality of Lyapunov spectra" as $L(i/N)$ approximately takes the same form in a finite range of large i/N regardless of total energy and details of systems. Models investigated in this chapter are XY, DW, SW, LO and 3DFPU.

5.1 New universality of Lyapunov spectra

In this section, we show that new universality of Lyapunov spectra exists in moderately chaotic systems in the thermodynamic limit ($N \to \infty$) through giving the following three results. (i) The degrees of freedom $N = 4^3$ is high enough to reach the thermodynamic limit for Lyapunov spectra. (ii) Forms of Lyapunov spectra are invariant with respect to energy in each of the four models which are XY, DW, SW and LO in a finite range of large i/N. (iii) The invariant forms of the four systems are in good agreement, and they are not approximated by the straight line. Here we conclude that new universality of Lyapunov spectra is found. After that, we study Lyapunov spectra of 3DFPU model to detect condition yielding the universality.

Lyapunov spectra for XY model are shown in Fig.5.1(a) in which points and dots represent that the degrees of freedom are $N = 4^3$ and 10^3 respectively. Numbers in the figure are values of energy density E/N. The Lyapunov spectra do not correspond with each other even though they have the same energy density.

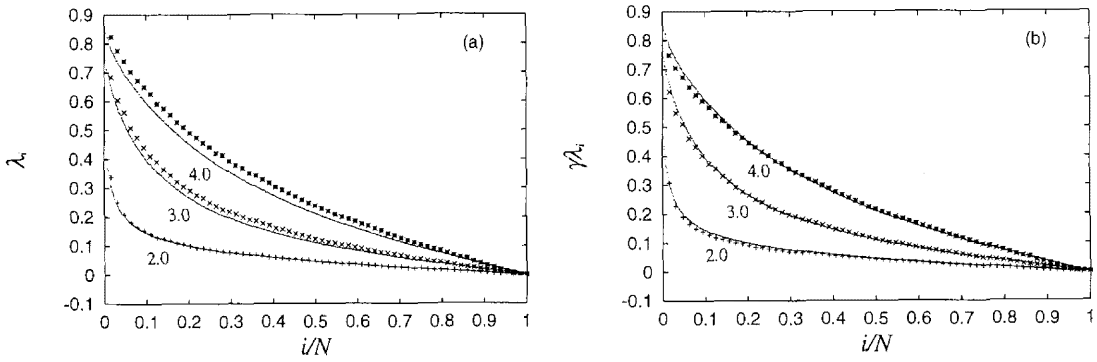

(a) non-scaled (b) scaled

Figure 5.1: Dependence on degrees of freedom N. Points and dots are Lyapunov spectra for $N = 4^3$ and 10^3 respectively. Numbers in the figure represent values of energy density E/N. (a) Non-scaled. (b) Vertical axis is scaled for $N = 4^3$ and the scale factor $\gamma = 1/1.1$ for all values of energy. In each energy, scaled Lyapunov spectrum for $N = 4^3$ is in good agreement with one for $N = 10^3$.

Let us note that the form of Lyapunov spectrum $L(i/N)$ is determined by ratios between Lyapunov exponents λ_i rather than their absolute values. Accordingly, we may uniformly scale Lyapunov spectrum up or down from $L(i/N)$ to $\gamma L(i/N)$, where γ is arbitrarily picked for each spectrum. To multiple $L(i/N)$ by γ corresponds to change time scale from t into t/γ. Scaled Lyapunov spectra are shown in Fig.5.1(b), and their forms holds regardless of degrees of freedom, where scale factors are $\gamma = 1/1.1$ and 1.0 for each spectrum in $N = 4^3$ and 10^3 respectively. Since the thermodynamic limit of Lyapunov spectra [LPR86, Rue82] exists, we suppose that the system reaches the thermodynamic limit even $N = 4^3$ concerning Lyapunov spectra. We therefore set $N = 4^3$, and use scaled Lyapunov spectra without comment hereafter.

Invariance of $L(i/N)$ with respect to energy is shown in Fig.5.2 for the four models. In each of the models, Lyapunov spectra are in good agreement among various values of energy in a range of large i/N in middle energy regime. Scale factor γ and the ranges of i/N where the invariance appears are arranged in Tables B.1 and B.2, respectively. We remark that the invariance breaks or is strictly limited in a narrow range of i/N when energy is too high or low, that are

$E/N = 100$ in XY and DW, and $E/N = 1.0$ in SW.

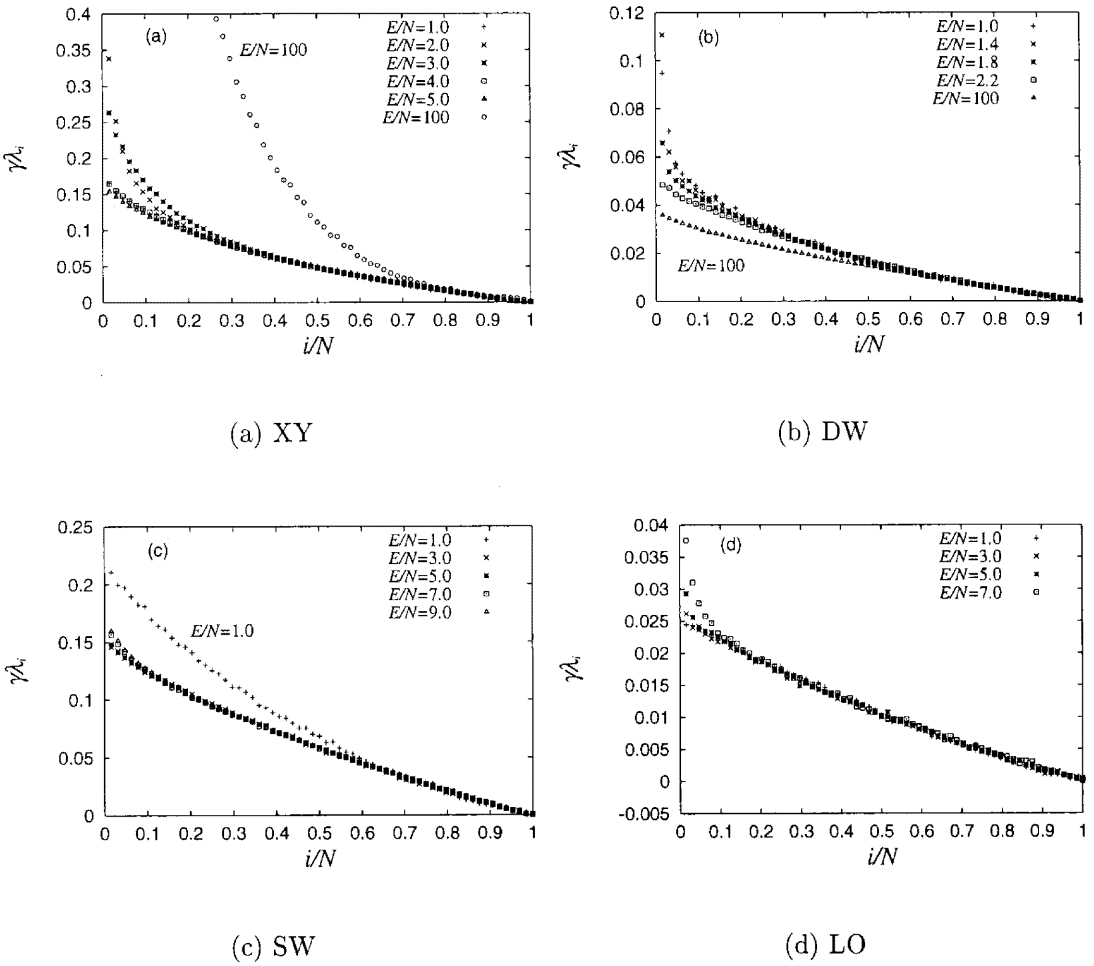

(a) XY (b) DW

(c) SW (d) LO

Figure 5.2: Lyapunov spectra for various values of energy in four Hamiltonian systems. (a) XY model. (b) DW model. (c) SW model. (d) LO model. Forms of Lyapunov spectra are the same in a range of large i/N in middle energy regime in each model. Scale factor γ and the range of i/N giving the invariant form are arranged in Tables B.1 and B.2.

Next we show the invariant forms of Lyapunov spectra of the four models together in Fig.5.3. Scale factor γ is arranged in Table B.3. The four spectra in Fig.5.3 coincide in a range of large i/N ($0.4 \lesssim i/N \leq 1$), while the straight solid line, which is obtained from random matrices, approximates them in a narrower range ($0.7 \lesssim i/N \leq 1$). That is, the invariant forms do not depend on details of models and are not straight, and consequently, Lyapunov spectra of the four models have universality which is different from the one obtained in fully

chaotic systems. The universality appears in moderately chaotic systems since it is yielded by the values of energy used in Fig.3.2, with which the systems are moderately chaotic.

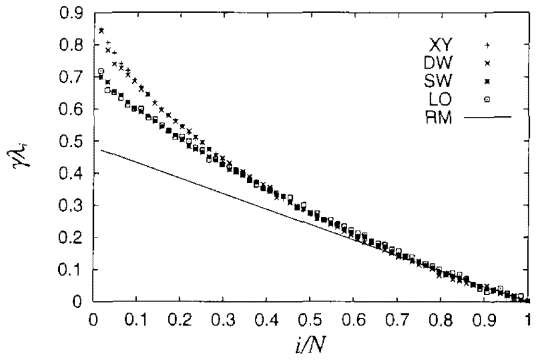

Figure 5.3: Universal behaviour of scaled Lyapunov spectra of four models. The Lyapunov spectra coincide well among the four models in a range of large i/N, namely $0.4 \lesssim i/N \leq 1$, and they are not approximated by the straight line, which approximates them only in the range of $0.7 \lesssim i/N \leq 1$. The straight line is obtained from random matrices. Scale factor γ is arranged in Table B.3.

5.2 3DFPU model and quadratic interactions

To probe what conditions yield the universality, we study 3DFPU model with various values of energy density E/N and coupling constant k (see Eq.(3.8)). Lyapunov spectra for 3DFPU model are shown in Fig.5.2 with a Lyapunov spectrum for XY model belonging in the universality, and they are classified into group C and group S. Group C includes the universal Lyapunov spectrum which is in good agreement with curved three spectra for 3DFPU, and other spectra for 3DFPU are straight and belong to group S. The classification is arranged in Table 5.1 with respect to k and E/N. Lyapunov spectra show curved forms when k is large and E/N is low, we hence conjecture that quadratic terms of potential function are dominant rather than quartic terms when the universality appears.

This conjecture is verified by taking ratios between time averages of U_2 and U_4, namely $\overline{U_2}/\overline{U_4}$, where

$$U_2 = \sum_{<ij>} \frac{k}{2}(q_i - q_j)^2, \tag{5.1}$$

$$U_4 = \sum_{<ij>} \frac{1}{4}(q_i - q_j)^4, \tag{5.2}$$

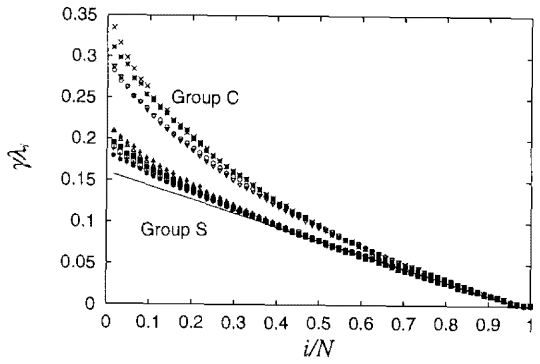

Figure 5.4: Lyapunov spectra in 3DFPU model. They are classified into group C and group S. Group C includes the universal spectrum which is in agreement with three spectra for 3DFPU, while group S consists of six spectra for 3DFPU which are straight. The straight line is a guide for eyes. The classification is arranged in Table 5.1 with respect to k and E/N. Scale factor γ shown in Table B.4.

Table 5.1: Behaviour of Lyapunov spectra in 3DFPU model. k and E/N are coupling constant and energy density, respectively. The sign S means straight behaviour of the Lyapunov spectrum, while the sign C curved behaviour. The forms of curved Lyapunov spectra are in good agreement with the universal form.

$k \setminus E/N$	1.0	2.0	3.0
0.4	S	S	S
0.7	C	S	S
1.0	C	C	S

Table 5.2: Ratios between time averages of the quadratic term U_2 and the quartic terms U_4 of potential function in 3DFPU model. We subtract 1.50 from each of the ratios to make a threshold clear, namely values arranged in this table are $\overline{U}_2/\overline{U}_4 - 1.50$. The positive values are found at the places where the sign C appears in Table 5.1.

$k \setminus E/N$	1.0	2.0	3.0
0.4	-0.60	-0.91	-1.02
0.7	0.33	-0.33	-0.62
1.0	1.55	0.37	-0.09

and

$$\overline{U}_n = \lim_{T\to\infty} \frac{1}{T} \int_0^T dt U_n(t), \qquad (n = 2, 4). \tag{5.3}$$

The ratios are arranged in Table 5.2, and they are large at the places where the sign C appears in Table 5.1. Consequently, the conjecture is verified.

5.3 Short summary

we numerically investigated Lyapunov spectra $\{\lambda_i\}$ for five Hamiltonian systems with many degrees of freedom. We showed existence of universality of Lyapunov spectra, which is defined as Lyapunov spectra approximately take the same form regardless of energy and details of systems. The universality gives a curved form for Lyapunov spectra, and hence it is different from the one obtained in fully chaotic systems.

A feature of the new universality is that it appears in a finite range of large i/N ($0.4 \lesssim i/N \leq 1$), where N is the number of degrees of freedom, and accordingly, properties depending on energy or details of models affect forms of Lyapunov spectra only in the range of small i/N where is out of the universality. In other words, we have only to focus on the range of small i/N when we are interested in such individual properties. When the universality appears potential function is dominated by quadratic terms rather than higher order terms.

We therefore suppose that harmonic motion in high dimensional subspace of phase space is the cause of the universality, where the high dimensional subspace corresponds to the finite range of i/N.

We geometrically interpret the harmonic (regular) motion and that the universality appears in a finite range of i/N as follows. Structure of phase space must consists of chaotic sea and debris of k-dimensional tori, where $k \leq N$ and k may change for each torus. Here k-dimensional torus is, roughly speaking, direct product of T^k and $(N-k)$-dimensional instability, which is hyperbolic or complex. Note $k = N$ is KAM torus. In the next chapter we construct a geometrical model with these considerations.

Chapter 6

A Geometrical Model for Stagnant Motion

In the previous section it is suggested that there exist the universal structure in a high-dimensional subspace of phase space, where the subspace corresponds to a range of large i/N in which the universal form of Lyapunov spectra appears. We must consider not only N-dimensional tori (KAM tori) but k ($\leq N$)-dimensional tori to construct a geometrical model of the phase space. In this chapter, we propose a geometrical model which represents hierarchical structure of the phase space, and which is based on fixed points of the Poincaré mapping. The model is an extension of Aizawa model to many degrees of freedom, while Aizawa model is based on KAM tori. The extended model assumes that sticky zones exist around fixed points of the Poincaré mapping even if fixed points are not fully elliptic. In other words, in systems with N degrees of freedom, motion is assumed to be trapped for a while around less than N dimensional tori, too. On the other hand, the model does not assume exact self-similarity which is assumed in Aizawa model.

6.1 Types of fixed points

We consider a Poincaré mapping F and its fixed points instead of a Hamiltonian flow and its periodic orbits. We set the number of degrees of freedom to n for the Poincaré mapping which has $2N-2$ dimensional Poincaré section, where N is the number of degrees of freedom of the Hamiltonian dynamics (i.e. $n = N-1$). We can construct the model based on periodic points of F with period-k by using F^k instead of F.

Local structure around fixed points is built from a combination of the three elementary types: elliptic, hyperbolic and vortex types, for which the eigenvalues of the Jacobian of F are $(e^{i\omega}, e^{-i\omega})$, $(r, 1/r)$ and $(re^{i\omega}, re^{-i\omega}, e^{i\omega}/r, e^{-i\omega}/r)$ respectively, where both ω and r are real [Arn68a]. Flows of mapping around the fixed

points are shown in Fig.6.1. The local structure is constructed as direct products of these three types.

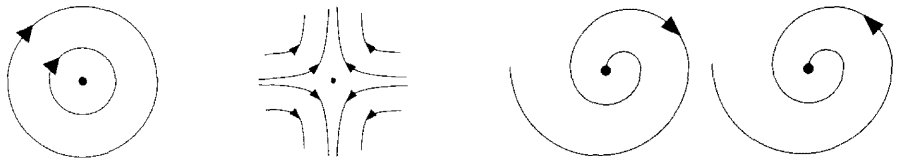

(a) Elliptic (b) Hyperbolic (c) Vortex

Figure 6.1: Flows of mapping around fixed points of elliptic, hyperbolic and vortex types.

We assume that there is no vortex type structure for simplicity. Generalication including the vortex type is easy and will be given in Ref. [YK98b]. Then local structure around a fixed point is constructed by elliptic and hyperbolic types structure, and there are $n+1$ varieties of fixed points: direct products of $n-i$ elliptic type and i hyperbolic ($i = 0, 1, \cdots, n$). We define index of a fixed point as i. For instance, a fully elliptic fixed point is index-0 and a fully hyperbolic is index-n.

6.2 Geometrical model

Let us introduce a geometrical model with the following assumptions:
(G-1) Hierarchical structure is constructed by fixed points of a Poincaré mapping in the phase space.
(G-2) Every type of fixed points has a sticky zone around it, even if it is not fully elliptic.
We calculate volumes of each level of hierarchy and derive a master equation with some assumptions. The number of the level is put in order by volume, and the base level is level-0. We assume that the regions of level-$(l+1), (l+2), \cdots$ are surrounded by the region of level-l. The schematic picture of this model is described in Fig.6.2.

Let us introduce notation of quantities which are used later:

$N_{l,i}$: number of fixed points of level-l, index-i,
$V_{l,i}$: volume of a sticky zone around a fixed point of level-l, index-i,
$\hat{N}_l$: total number of fixed points of level-l,
$\hat{V}_l$: total volume of sticky zones of level-l,

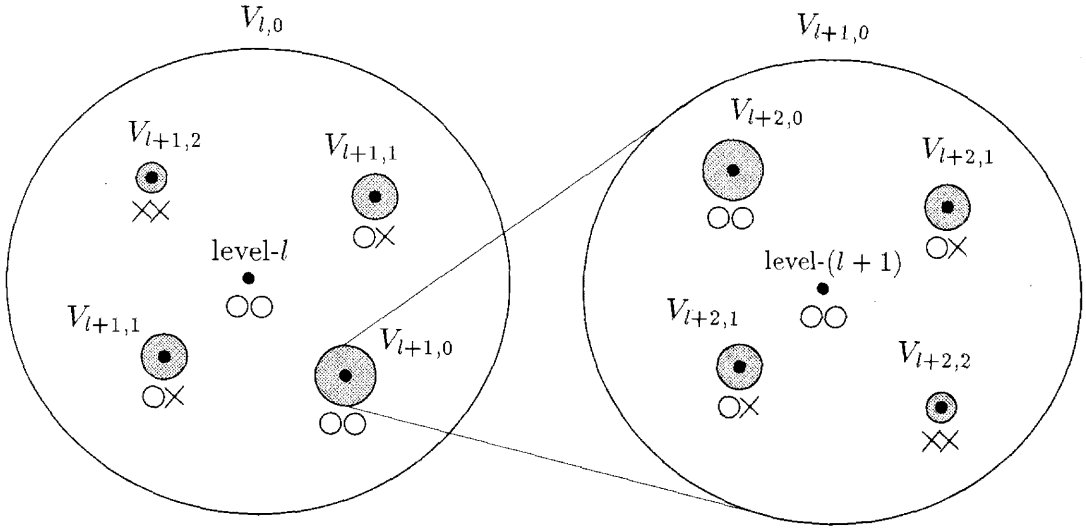

Figure 6.2: Schematic picture of the hierarchical structure of phase space. In this picture we assume the system size to be $n = 2$. Black points are fixed points. Circle and cross under the fixed points represent elliptic and hyperbolic elementary types, respectively. The double circle, for instance, implies that the structure around the fixed point is direct product of two elliptic types, namely index-0. Let us focus on the left half of this figure. The fixed point at the centre, whose index is 0, belongs to level-l, and the other four fixed points belong to level-$(l+1)$. The sticky zone of the fixed points at the centre is inside of the biggest circle except for the shaded areas. The structure of a shaded area is similar to the one inside of the biggest circle. Level-$(l+2)$ fixed points exist around level-$(l+1)$ fixed points, with a similar situation as the right half, which is magnification around a fixed point with level-$(l+1)$ and index-0.

$\rho_{l,i}$: number of sets of fixed points of level-$(l+1)$,
which surround a fixed point of level-l, index-i.

Here we assumed:
(G-3) Fixed points have the same volume $V_{l,i}$ if their level and index are the same.
The meaning of $\rho_{l,i}$ is clarified in the following.

(Fact): A fixed point of level-l and index-i is surrounded by $\rho_{l,i}({}_{n-i}C_j)$ fixed points of level-$(l+1)$ and index-$(i+j)$, where $j = 0, 1, \cdots, n-i$, and $\rho_{l,i}$ is a positive integer.

This fact is an extension of the Poincaré-Birkhoff theorem [LL92] for many degrees of freedom [Arn68b]. Using this fact, we write the recursion formula for $N_{l,i}$ as

$$N_{l+1,i} = \sum_{k=0}^{i} \rho_{l,k} N_{l,k} ({}_{n-k}C_{i-k}). \tag{6.1}$$

THe total number $\hat{N}_l$ and volume $\hat{V}_l$ of the level-l sticky zones are

$$\hat{N}_l = \sum_{i=0}^{n} N_{l,i}, \qquad \hat{V}_l = \sum_{i=0}^{n} N_{l,i} V_{l,i}. \tag{6.2}$$

Note that the hierarchical structure assumed in (G-1) is not exactly self-similar, which is assumed in Aizawa model. The reason is as follows. The exact self-similarity in $n = 1$ is based on that $N_{l,0} = \rho^l N_{0,0}$, and the Eq.(6.1) can yield the self-similarity if we take $\rho_{l,0} = \rho$. However, in $n > 1$, there are many types of fixed points considered in this model, and the number of the fixed points is not power type of level-l, i.e. $N_{l,i} \neq (\rho_{l,i})^l N_{0,i}$. The hierarchy is therefore not self-similar in $n > 1$. Afterwards, we show that self-similarity is asymptotically recovered in deep levels.

6.3 Master equation

To observe motion among levels, we introduce a master equation with the following three assumptions:
(M-1) Systems are ergodic.
(M-2) Transitions from level-l are limited to level-$(l-1)$, l and $(l+1)$.
(M-3) Transitions among levels are Markovian.
From (M-1), probability being level-l in equilibrium, P_l^{eq}, is proportional to volume $\hat{V}_l$:

$$P_l^{\mathrm{eq}} \propto \hat{V}_l. \tag{6.3}$$

We assume detailed balance to fix the transition probability $w_{m,l} \equiv w\{l \to m\}$. Then

$$w_{l,m} P_m^{\mathrm{eq}} = w_{m,l} P_l^{\mathrm{eq}}. \tag{6.4}$$

From (M-2) and Eqs.(6.3) and (6.4), transition probabilities are written as

$$w_{m,l} = \begin{cases} c\hat{V}_{l-1}, & (m = l-1) \\ 1 - w_{l-1,l} - w_{l+1,l}, & (m = l) \\ c\hat{V}_{l+1}, & (m = l+1) \\ 0. & (\text{otherwise}) \end{cases} \tag{6.5}$$

The factor c is independent of the level, and we set $c = 1/(2(\hat{V}_0 + \hat{V}_2))$. By using these transition probabilities, the master equation is written as

$$P_l(t+1) = \sum_m w_{l,m} P_m(t), \tag{6.6}$$

where $P_l(t)$ is the probability of being on level-l at step t.

6.4 Total volume of sticky zones

We show $\hat{V}_l$ as a function of level for various system size n in Fig.6.3. Figure 6.3 shows that $\hat{V}_l$ is exactly exponential when $n = 1$ as a result of exact self-similarity. For systems with $n > 1$ the phase space is not exactly self similar and $\hat{V}_l$ is not necessarily proportional to v^{-l}, where v is an appropriate real number. Figure 6.3 shows $\hat{V}_l \propto v^{-l}$ for large level-l, and hence self-similarity is asymptotically recovered in deep levels.

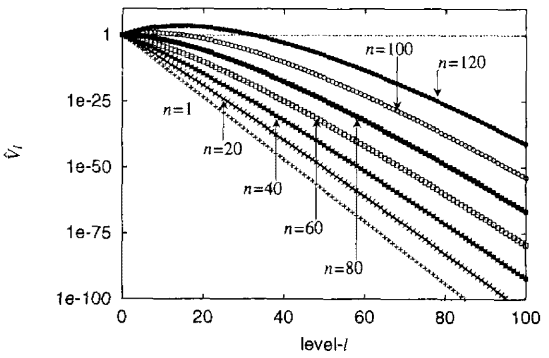

Figure 6.3: Level dependence of total volume $\hat{V}_l$. Numbers in this figure are degrees of freedom of Poincaré mapping. $b = 30$.

6.5 Residence time distribution

We numerically calculated residence time distributions based on our model Eq.(6.6) and examined if it obeys a power law. The residence time distribution $R(t)$ is the

probability that motion extende to levels shallower than level-$l_{\rm th}$ for the first time with initial level being l_{th} at $t = 0$. We obtain $R(t)$ from the following transition probabilities and initial condition:

$$w_{m,l_{\rm th}-1} = 0 \quad (m = l_{\rm th} - 1, l_{\rm th}, l_{\rm th} + 1), \qquad P_l(t = 0) = \delta_{l,l_{\rm th}}. \tag{6.7}$$

Here $\delta_{l,l_{\rm th}}$ is Kronecker's delta. Then we have

$$R(t) = P_{l_{\rm th}-1}(t). \tag{6.8}$$

If $R(t)$ is of a power type rather than an exponential, motion among levels is stagnant. That is, motion in phase space is trapped in small areas, which correspond to deep levels of hierarchy, and long time correlation remains.

Parameters which must be given are assumed as follows:

$$V_{l,i} = b^{-(l+i)}, \qquad \rho_{l,i} = 2, \qquad l_{\rm th} = 1,$$

$$N_{0,0} = 1 \quad \text{and} \quad N_{0,i} = 0. \quad (i > 0)$$

Sticky zones become small as hyperbolic components increases, and an essential point of this is that $V_{l,i}$ depends on the index. We assumed that the volume of a sticky zone $V_{l,i}$ decays as b^{-i} with respect to the index-i of the fixed point, since local structure near fixed points is constructed by direct products. Other forms of $V_{l,i}$, for instance $V_{l,i} = b^{-l}\tilde{b}^{-i}$ and $V_{l,i} = \exp[-(l + i^{\alpha}) \ln b]$, give similar results to $V_{l,i} = b^{-(l+i)}$ with appropriate values of parameters. The form of $V_{l,i}$ determines which index is dominant in $\hat{V}_l$.

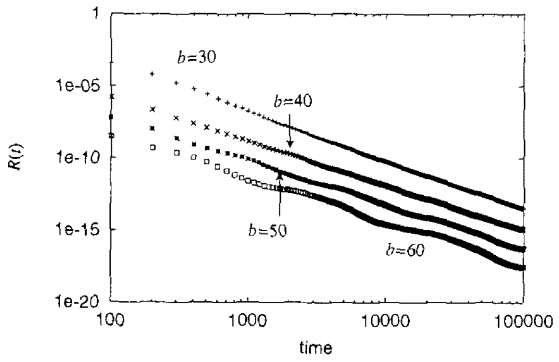

Figure 6.4: Residence time distributions for various values of the scale factor b. Here $n = 80$. The magnitude of the longitudinal axis is multiplied by $10^{-1}, 10^{-2}$ and 10^{-3} for $b = 40,\ 50$ and 60, respectively.

The residence time distribution $R(t)$ is shown in Fig.6.4 for $n = 80$ and various values of b. When b is small ($b = 30, 40$) $R(t)$ is of a power type. Namely, we

have

$$R(t) \sim t^{-\beta}, \quad \text{where } \beta = \begin{cases} 3.4 & (b = 30) \\ 3.1 & (b = 40) \end{cases} . \tag{6.9}$$

Since $R(t)$ is of a power type, stagnant motion occurs among levels. The stagnant motion is also observed when $n = 1$, and hence our model Eq.(6.6) is consistent with Aizawa model. The values of β are also consistent with those obtained in area preserving mappings which are models of physical systems and give $1.5 \leq \beta \leq 3$. [Kar83, CS84, IYS91] As far as we know, β has not been calculated in Hamiltonian systems with many degrees of freedom. Appearance of oscillating behaviour for $b = 50$ and $b = 60$ is caused by the weakness of effects of the hierarchy, which become weaker as b increases because large b implies that level-$(l+1)$ is small compared with level-l.

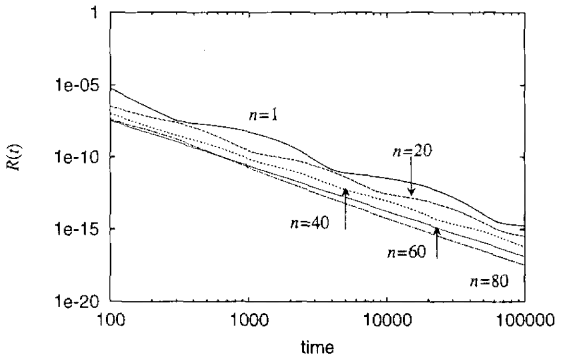

Figure 6.5: Dependences of residence time distributions with fixed $b = 30$. The magnitude of longitudinal axis is multiplied by 10^{-1}, 10^{-2}, 10^{-3} and 10^{-4} for $n = 20$, 40, 60 and 80, respectively. The distributions are closer to a power type as n increases.

We display the residence time distribution $R(t)$ for various system size n in Fig.6.5, where power law behavior of $R(t)$ is clearly seen. Oscillations found for small n gradually decay as n becomes large, and the distributions are close to a power type as n increases. This is an effect of the many degrees of freedom and indicates that fine tuning of parameters is not necessary to observe $1/f$ spectra in systems with many degrees of freedom.

6.6 Dominant index

Finally we show that "trunk" of tree of hierarchy is not necessarily fully elliptic fixed points (index-0), where we define the word "trunk" as index at which $N_{l,i}V_{l,i}$ takes the maximum. In Fig.6.6 $N_{l,i}V_{l,i}$ is shown as a function of index-i for various

level-l. The "trunk" of level-20 is index-40 for instance. The "trunk" shifts to larger index-i and converges on a certain index as level-l becomes deeper. Which index is selected as the convergent "trunk" is decided by details of each Hamiltonian, and it is around index-77 in our case. The "trunk" dominates $\hat{V}_l$ and mainly constructs tree of hierarchy, and hence rich hierarchical structure appears although KAM tori rapidly disappears as the system size n gets large.

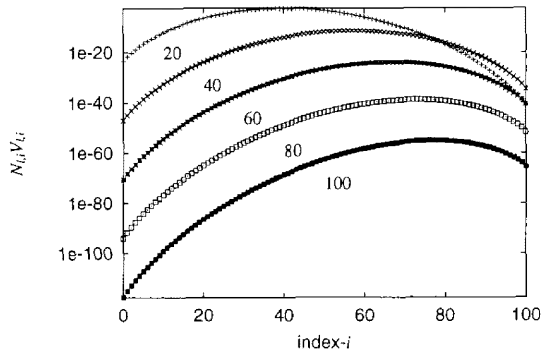

Figure 6.6: Volume of index-i fixed points in various level. $n = 100$. Longitudinal axis shows $N_{l,i}V_{l,i}$. Numbers in the figure represent depth of level-l. Index where the $N_{l,i}V_{l,i}$ takes the maximum is not necessarily zero, namely fully elliptic.

6.7 Short summary

To understand the global structure of phase space in systems with many degrees of freedom, we proposed a geometrical model of phase space, which is an extension of Aizawa's model to systems with many degrees of freedom. We assumed hierarchical structure of phase space which is constructed by fixed points of Poincaré mapping. We also assumed existence of sticky zones around the fixed points even if the fixed points are not fully elliptic. Accordingly, exact self-similarity of phase space is not assumed. The self-similarity is, however, asymptotically recovered in deep levels in the extended model. We derived a master equation from the model, and found that residence time distributions are of a power type, that is, stagnant motion among levels occurs. We hence suppose that the model catches essence of the global structure in systems with many degrees of freedom. The power law behaviour becomes clearer as the system size becomes large when we fixed parameters except for degrees of freedom. This is an effect of high-dimensionality. Another effect is that the hierarchical structure is generally dominated by non-fully elliptic fixed points, namely non-KAM tori.

Chapter 7

Summary and discussions

We investigated Hamiltonian systems with many degrees of freedom. Hamiltonian systems with more than one degrees of freedom are generally chaotic, that is, motion exponentially loses initial information and it is unpredictable accordingly. In spite of the exponential loss, we can understand global structure of phase spaces from theories and numerical experiments, and dynamical properties like long time tail reflect the global structure. We are therefore interested in the global structure, in particular, which are not affected by details of systems.

We classified Hamiltonian systems into four classes: integrable, nearly integrable, moderately chaotic and fully chaotic systems. We have understood global structures in integrable, nearly integrable and fully chaotic systems. The global structures consist of tori and chaotic seas in integrable and fully chaotic systems respectively, and they do not yield long time tail. Hierarchical structure based on KAM tori obtained in nearly integrable systems is usually used to understand the long time tail in systems with two degrees of freedom, which is the lowest degrees of freedom to be chaotic. However, assuming the hierarchical structure is not practical in systems with many degrees of freedom since it is believed that KAM tori rapidly disappear as system size gets large. In this thesis, the class of moderately chaotic systems is thus introduced whose strength of chaos is stronger and weaker than nearly integrable and fully chaotic systems, respectively.

The main purposes of this thesis are to reveal global structure in this class and to understand the long time tail from the structure.

Although the existence of moderately chaotic systems is not obvious, we showed it in Chap.3. We introduced six Hamiltonian systems, and in these systems, we calculated local Lyapunov exponents, a power spectrum and Lyapunov spectra in middle energy regime. Local Lyapunov exponents do not show intermittency which appears in nearly integrable systems, and hence we concluded that the systems are not nearly integrable. Power spectra and Lyapunov spectra are available to show that systems are not fully chaotic. A power spectrum calculated in one of the six systems is neither white nor Lorentzian, and accordingly, correlation in the system is not neither δ- nor exponential function. The system

is therefore not fully chaotic. We calculated Lyapunov spectra in the other five systems, and the Lyapunov spectra are not straight while they are universally straight in fully chaotic systems. The five systems are also not fully chaotic. Consequently, all of the six Hamiltonian systems are moderately chaotic.

Next, we investigated an interesting phenomenon occurring in a moderately chaotic system in Chap.4. We took one of the six systems which is a model of second order phase transition. We numerically integrated the equations of motion, and observed slow relaxation of order parameter at the critical point. As far as I know, this is the first time to show the slow relaxation from direct integration of equations of motion.

The dynamical properties of critical phenomena have been studied by using phenomenological theories, statistical mechanics, Monte Carlo simulations and so on. They require some assumptions to obtain temporal evolutions, in particular, they assume that state is at or around thermal equilibrium. Relaxation to the equilibrium is slow at the critical point, and hence validity of the assumption is not obvious. Hamiltonian equations of motion directly give temporal evolution of system without any assumptions even at the critical point, and hence they are useful to study dynamical properties of phase transition. The slow relaxation in Chap.4 suggests fruitfulness to study critical phenomena as Hamiltonian dynamics.

In Chap.5 we analised Lyapunov spectra in the six Hamiltonian systems with moderate strength of chaos. Although Lyapunov spectrum is usually used to study instability of a sample orbit, it is useful to discuss structure of phase space since it includes information of the whole degrees of freedom. In particular, universal behaviour of Lyapunov spectra must reflect universal structure of phase space, in which we are interested. For instance, fully chaotic systems universally show straight behaviour.

We discovered universal behaviour of Lyapunov spectra $\{\lambda_i\}$, which differs from the straight one obtained in fully chaotic systems. A feature of the new universality is to appear only in a finite range of large i/N, where N is the number of degrees of freedom. Let us use the letter k $(< N)$ to represent the width of range where the universality appears, i.e. the universality appears in $N-k < i \leq N$. Phase spaces therefore have universal structure in $2k$-dimensional subspaces in moderately chaotic systems, while the whole dimensional phase space have universal structure of hierarchy in nearly integrable systems. The hierarchical structure consists of N-dimensional tori, namely KAM tori, and hence the new universality suggests that we must consider k-dimensional tori to understand the universal structure in moderately chaotic systems. Here, roughly speaking, k-dimensional tori is built by direct products of T^k and $(N-k)$-dimensional unstable space. The suggestion is supported by that quadratic terms of potential function dominate higher order terms when the new universality of Lyapunov spectra appears.

With the aid of the suggestion, we constructed a geometrical model in Chap.6.

The model is an extension of Aizawa model to high-dimensional and moderately chaotic systems. Aizawa model is based on hierarchical structure consisting of KAM tori, and the basic idea of Aizawa model is to assume existence of sticky zones around KAM tori. In the sticky zones motion is assumed to be stagnant since it goes to depth of the hierarchy and is trapped in local areas of phase space.

The idea of the extension is to assume the existence of sticky zones around any dimensional tori, too. The extended model successfully yield long time tail as Aizawa model even if k ($< N$)-dimensional tori is dominant in deep levels of hierarchy with respect to volume of sticky zones around them, in other words, even if enough KAM tori do not survive. The extended model hence conceptually describes global structure of phase spaces in moderately chaotic systems, and the structure is mainly built by k-dimensional tori instead of KAM tori.

The extended model includes some free parameters, and hence it supports wide classes of chaotic systems by appropriately selecting values of the parameters. For instance, the model represents nearly integrable systems by selecting the parameters as N-dimensional tori dominate the volume of sticky zones.

We remark that moderately chaotic systems do not exist in systems with two degrees of freedom. The reason is as follows. The geometrical model considers structure of Poincaré section, and only elliptic and hyperbolic fixed points exist on the section which correspond 2- and 1-dimensional tori. Poincaré-Birkhoff theorem states that the numbers of the elliptic and hyperbolic fixed points are the same, and volume of sticky zones around an elliptic fixed point is bigger than one around a hyperbolic. Consequently, in systems with two degrees of freedom, 2-dimensional KAM tori are always dominant, that is, systems are nearly integrable when hierarchy appears.

This work must be extended to a lot of directions as follows.

First, we must check whether universality of Lyapunov spectra includes the class of systems which have long range force given by Coulomb's low, gravitation and so on, while the six Hamiltonian systems considered in this thesis have bounded potential functions.

Second, we have not clarified the origin of the universal form of Lyapunov spectra. For instance, there is a problem why the form is downward convex. To reveal the origin of the form must provide us further understanding of global structure. Let us give geometrical and analytical approaches to the origin.

A geometrical approach uses resonance of instability along an orbit. Negative curvature of potential function induces positive Lyapunov exponent. On the other hand, even the curvature is always positive, resonance of instability along a sample orbit gets the largest Lyapunov exponent to be positive [Pet93]. Here let us assume this resonance theory can be extended not only to the largest Lyapunov exponent but to all the exponents. If the resonances are yielded by k-dimensional tori, namely by harmonic motion in high-dimensional subspaces of phase space, then universality of Lyapunov spectra may be obtained because harmonic motion is independent of details of models.

An analytical approach is to calculate decay rate spectrum of the harmonic motion. In a dissipative system, behaviour of Lyapunov spectrum agrees with the decay rate spectrum of the linear fluctuation modes from the stationary solution [IM86]. This suggests that to analyse decay rate spectrum is useful to understand behaviour of Lyapunov spectrum. Hamiltonian systems are regarded as dissipative systems when we observe only subspaces of phase spaces, and hence the decay rate spectrum must be useful because the new universality appears only in high-dimensional subspaces of phase spaces.

Third, we must consider motion in a level of hierarchy, too. In the extended geometrical model we reduced such motion to volume of sticky zones, and we have not discussed dynamical properties of transition between sticky zones belonging to the same level. The "horizontal" motion (inner level) with the "vertical motion (inter-level) will richly describe structure of phase space.

Finally we mention an interesting remark. Usually it is regarded that dynamics is determined by a degrees of freedom corresponding to the largest Lyapunov exponent, since motion is the most unstable for the direction pointed by the largest Lyapunov vector. However, following the geometrical model proposed in this thesis, we reach the understanding that slow dynamics like long time tail is determined by degrees of freedom corresponding to directions having weaker instability and hidden by the most unstable one. This understanding is also obtained in a dissipative system [HKT97].

The deep degrees of freedom never dead in phase space, but they slowly drive nature.

Appendix A

Lyapunov exponents and spectrum

A.1 The definition

Lyapunov spectrum indicates linear instability along an orbit, and it is a set of Lyapunov exponents $\{\lambda_1, \lambda_2, \cdots, \lambda_D\}$, where the system has D-dimensional phase space. The Lyapunov exponents are usually arranged as the decreasing order $\lambda_1 \geq \lambda_2 \geq \cdots \geq \lambda_D$.

Let us describe the definition of Lyapunov spectrum. We introduce the squared Jacobi matrix;

$$M(t) \equiv \frac{\partial X(t)}{\partial X(0)}, \tag{A.1}$$

where $X(t) = (x_1(t), x_2(t), \cdots, x_D(t))$ is a D-dimensional tangent vector. Lyapunov spectrum is defined from the eigenvalue spectrum of ${}^tM(T)M(T)$ as

$$\begin{aligned} \{\mathrm{e}^{2\lambda_1 T}, \mathrm{e}^{2\lambda_2 T}, \cdots, \mathrm{e}^{2\lambda_D T}\} &= \text{eigenvalue spectrum of } {}^tM(T)M(T) \\ &\quad \text{as } T \to \infty, \end{aligned} \tag{A.2}$$

where ${}^tM(T)$ is the transposed matrix of $M(T)$.

The first exponent λ_1 is usually called Lyapunov exponent, and Lyapunov exponent represents the asymptotic expansion rate of an infinitesimal line segment long an orbit. The summation $\lambda_1 + \lambda_2$ represents asymptotic expansion rate of an infinitesimal area element. Similarly, the summation up to the k-th Lyapunov exponent, $\sum_{i=1}^{k} \lambda_i$, represents the asymptotic expansion rate of k-dimensional volume element $V_k(t)$, i.e.

$$V_k(t) \sim \exp\left(t \sum_{i=1}^{k} \lambda_i\right) \text{ in the limit of } t \to \infty. \tag{A.3}$$

The sign of Lyapunov exponent indicates whether the orbit is chaotic or not, that is,

$$\begin{array}{lll} \lambda_1 > 0 & \Rightarrow & \text{chaotic}, \\ \lambda_1 \leq 0 & \Rightarrow & \text{regular}. \end{array} \tag{A.4}$$

A.2 In symplectic systems

In symplectic systems like Hamiltonian systems and Poincaré mappings, Jacobi matrix is defined as

$$M(t) \equiv \frac{\partial(p(t), q(t))}{\partial(p(0), q(0))}, \tag{A.5}$$

and it is symplectic. A matrix M is symplectic if and only if M satisfies the following equation;

$${}^tMJM = J, \tag{A.6}$$

where

$$J \equiv \begin{pmatrix} 0 & -1_N \\ 1_N & 0 \end{pmatrix}, \tag{A.7}$$

and 1_N is the unit matrix of $N \times N$. Direct calculation gives

$$J^{-1} = -J \qquad {}^tJ = -J. \tag{A.8}$$

Let us show that Lyapunov exponents have the following relations in symplectic systems;

$$\lambda_{2N-j+1} = -\lambda_j, \tag{A.9}$$

where $2N = D$ and N is the number of degrees of freedom. The Eq.(A.9) is shown as follows.

From the definition of symplectic matrix, Using Eqs.(A.6) and (A.8), ${}^tMM$ is rewritten as follows

$$\begin{aligned} {}^tMM &= -J(J^tMJ)(JMJ)J \\ &= -J(-M^{-1})(-{}^tM^{-1})J \\ &= -J({}^tMM)^{-1}J. \end{aligned} \tag{A.10}$$

Suppose we have an eigenvector v of the symmetric matrix ${}^tMM$, in accordance with the definition of Lyapunov exponents;

$${}^tMMv = \mathrm{e}^{2\lambda T}v. \tag{A.11}$$

We substitute Eq.(A.10) for Eq.(A.11), then

$$\begin{aligned} -J({}^tMM)^{-1}Jv &= \mathrm{e}^{2\lambda T}v, \\ ({}^tMM)^{-1}Jv &= \mathrm{e}^{2\lambda T}Jv, \\ ({}^tMM)^{-1}Jv &= \mathrm{e}^{-2\lambda T}Jv. \end{aligned} \tag{A.12}$$

That is, Jv is also an eigenvector of the matrix ${}^tMM$ with eigenvalue $\mathrm{e}^{-2\lambda T}$. Consequently, if there is a Lyapunov exponent λ, then $-\lambda$ is also a Lyapunov exponent in symplectic systems.

If a system has m integrals then $2m$ Lyapunov exponents take zero;

$$\lambda_{N-m+1} = \cdots = \lambda_N = \lambda_{N-1} = \cdots = \lambda_{N+m} = 0. \tag{A.13}$$

In integrable systems all the Lyapunov exponents take zero since there are N integrals. The N-th and $(N+1)$-th Lyapunov exponents are always zero even in chaotic systems since Hamiltonian itself is an integral.

Note that we can not judge whether a system is integrable or not by using Lyapunov exponents. Lyapunov exponents are defined for an orbit, and they take zero when the orbit runs on a KAM torus if the system is not integrable.

A.3 To numerically calculate Lyapunov spectrum

Finally, we describe a concrete process to numerically calculate Lyapunov spectrum. Let us consider a dynamical system

$$\dot{x} = f(x), \tag{A.14}$$

where $f = (f_1, f_2, \cdots, f_D)$. Lyapunov spectrum represents linear instability, and it is hence calculated from linearized equation of motion,

$$\frac{\mathrm{d}}{\mathrm{d}t}(\delta x) = Df(x)\delta x, \tag{A.15}$$

where δx is a D-dimensional tangent vector. The (i,j) element of the $D \times D$ Jacobi matrix $Df(x)$ is

$$(Df(x))_{i,j} = \left(\frac{\partial f_i}{\partial x_j}(x)\right). \tag{A.16}$$

We must discretize Eq.(A.15) to integrate it on computers, and we obtain

$$\begin{aligned} \delta x^{t+1} &= \delta x^t + \tau Df(x^t)\delta x^t \\ &= (1_D + \tau Df(x^t))\delta x^t, \end{aligned} \tag{A.17}$$

where τ is a fixed time slice and the superscript represents discretized time; $t = 0, 1, 2, \cdots$. Calculation consists of the following four steps.

(i) At the initial time $t = 0$, we pick out a orthonormal set of D tangent vectors

$$\delta x^0 = \{\delta x_1^0, \delta x_2^0, \cdots, \delta x_D^0\}, \tag{A.18}$$

where the subscript is the number of vectors and δx^0 is a $D \times D$ squared matrix. The selection of initial tangent vectors is almost arbitrary, and probability of unsuitable selection is zero. That is understood from the step (iii).

(ii) We evolve the set of tangent vectors following Eq.(A.17), then the set of vectors becomes

$$\delta y^1 = \{\delta y_1^1, \delta y_2^1, \cdots, \delta y_D^1\}. \tag{A.19}$$

The set δy^1 is generally no longer orthonormal.

(iii) We orthonormalize the set δy^1 with Gram-Schmidt orthonormalization procedure. Let us write the orthogonalized and the orthonormalized sets as

$$\delta z^1 = \{\delta z_1^1, \delta z_2^1, \cdots, \delta z_D^1\}, \tag{A.20}$$

$$\delta x^1 = \{\delta x_1^1, \delta x_2^1, \cdots, \delta x_D^1\}, \tag{A.21}$$

respectively, then

$$\begin{array}{rclcrcl} \delta z_1^1 &=& \delta y_1^1, & & \delta x_1^1 &=& \delta z_1^1/||\delta z_1^1||, \\ \delta z_2^1 &=& \delta y_2^1 - \delta x_1^1(\delta y_2^1 \cdot \delta x_1^1), & & \delta x_2^1 &=& \delta z_2^1/||\delta z_2^1||, \\ & \cdots & , & & \cdots & & , \\ \delta z_D^1 &=& \delta y_D^1 - \sum_{j=1}^{D-1} \delta x_j^1(\delta y_D^1 \cdot \delta x_j^1), & & \delta x_D^1 &=& \delta z_D^1/||\delta z_D^1||. \end{array} \tag{A.22}$$

Using δx^t we repeat the process (i), (ii) and (iii).

(iv) Lyapunov exponents are asymptotic expansion rates, and hence we calculate them from the following equations;

$$\begin{aligned} \lambda_j(T) &\equiv \frac{1}{\tau T} \log \frac{||\delta z_j^T||}{||\delta x_j^{T-1}||} \frac{||\delta z_j^{T-1}||}{||\delta x_j^{T-2}||} \cdots \frac{||\delta z_j^1||}{||\delta x_j^0||} \\ &= \frac{1}{\tau T} \sum_{t=1}^{T} \log ||\delta z_j^t||, \end{aligned} \tag{A.23}$$

$$\lambda_j = \lim_{T \to \infty} \lambda_j(T). \tag{A.24}$$

Appendix B

Tables of scale factor γ

Table B.1: Scale factor γ in figure 5.2.

XY		DW		SW		LO	
E/N	γ	E/N	γ	E/N	γ	E/N	γ
1.0	3.4	1.0	6.0	1.0	12	1.0	1.0
2.0	1.0	1.4	2.4	3.0	2.65	3.0	1.2
3.0	1/2.6	1.8	1.4	5.0	1.6	5.0	1.4
4.0	1/5.0	2.2	1.0	7.0	1.2	7.0	1.95
5.0	1/5.5	100	1/11	9.0	1.0		
100	4.0						

Table B.2: Rough estimations of ranges of i/N where universal behaviour of Lyapunov spectra appears in four models.

Model	XY	DW	SW	LO
i/N	[0.4,1]	[0.31,1]	[0.16,1]	[0.11,1]

Table B.3: Scale factor γ in figure 5.3.

Model	XY	DW	SW	LO
E/N	6.0	2.0	3.0	3.0
γ	1.0	18	12.7	33

Table B.4: Scale factor γ in figure 5.2.

$k \setminus E/N$	1.0	2.0	3.0
0.4	1.0	0.75	0.66
0.7	1.7	0.91	0.74
1.0	2.25	1.4	0.92

Bibliography

[Aiz84] Y. Aizawa. "Symbolic dynamics approach to the two-dimensional chaos in area preserving maps: a fractal geometrical model". *Prog. Theor. Phys.*, 71:1419–21, 1984.

[AKH+89] Y. Aizawa, Y. Kikuchi, T. Harayama, K. Yamamoto, M. Ota, and K. Tanaka. *Prog. Theor. Phys. Suppl.*, 98:36, 1989.

[AR95] M. Antoni and S. Ruffo. "Clustering and relaxation in Hamiltonian long-range dynamics". *Phys. Rev. E*, 52(3):2361–74, 1995.

[Arn63] V. I. Arnold. "Proof of a theorem of A.N.Kolmogorov on the invariance of quasi-periodic motions under small perturbations of the Hamiltonian". *Russ. Math. Surv.*, 18(5):9–36, 1963.

[Arn68a] V. I. Arnold. *"Ergodic problems in classical mechanics, Appendix 29"*. Benjamin-Cummings, Reading, Massachusetts, 1968.

[Arn68b] V. I. Arnold. *"Ergodic problems in classical mechanics, Appendix 33"*. Benjamin-Cummings, Reading, Massachusetts, 1968.

[Arn89] V. I. Arnold. *"Mathematical methods of classical mechanics"*. Springer-Verlag, New York, second edition, 1989. Chapter 10, Section 49.

[BHSO97] A. Baba, Y. Hirata, S. Saito, and I. Ohmine. "Fluctuation, relaxation and rearrangement dynamics of a model $(H_2O)_20$ cluster: non-statistical dynamical behavior". *J. Chem. Phys.*, 106:3329–37, 1997.

[CS84] B. V. Chirikov and D. L. Shepelyansky. "Correlation properties of dynamical chaos in Hamiltonian systems". *Physica D*, 13:395–400, 1984.

[Esc85] D. F. Escande. "Stochasticity in classical Hamiltonian systems: universal aspects". *Phys. Rep.*, 121:165–261, 1985.

[EW88] J.-P. Eckmann and C. E. Wayne. "Liapunov spectra for infinite chains of nonlinear oscillators". *J. Stat. Phys.*, 50:853–78, 1988.

[HI87] T. Hatori and H. Irie. *Prog. Theor. Phys. Suppl.*, 78:249, 1987.

[Hir] Y. Hirata. "An analytical method in chaotic Hamiltonian systems $\sim$ asymptotic expansions of invariant manifolds in 4-dimensional symplectic mappings". Master thesis, Nagoya Univ., 1997.

[HKT97] H. Hata, K. Kawano, and Y. Takada, October 1997. Private communication.

[IM86] K. Ikeda and K. Matsumoto. "Study of a high-dimensional chaotic attractor". *J. Stat. Phys.*, 44:955–83, 1986.

[Ina93] S. Inagaki. "Thermodynamic stability of modified Konishi-Kaneko system". *Prog. Theor. Phys.*, 90(3):577–84, 1993.

[IYS91] H. Irie, H. Yamaguchi, and M. Sato. *Physica D*, 54:20, 1991.

[Kar83] C. F. F. Karney. "". *Physica D*, 8:360, 1983.

[Kol54] A. N. Kolmogorov. *Dokl. Akad. Nauk SSSR*, 98:527, 1954.

[Kon94] T. Konishi. *"World in motion: chaos and order in Hamltonian dynamical systems with many degrees of freedom"*. PhD thesis, Univ. Tokyo, 1994.

[LL92] A. J. Lichtenberg and M. A. Lieberman. *"Regular and Chaotic Dynamics. Second Edition"*. Springer, 1992.

[LN92] P. Lochak and A. I. Neishtadt. "Estimates of stability time for nearly integrable systems with a quasiconvex Hamiltonian". *Chaos*, page 495, 1992.

[LPR86] R. Livi, A. Politi, and S. Ruffo. "Distribution of characteristic exponents in the thermodynamic limit". *J. Phys. A*, 19:2033–40, 1986.

[LPR87] R. Livi, A. Politi, and S. Ruffo. "Liapunov exponents in high-dimensional symplectic dynamics". *J. Stat. Phys.*, 46:147–60, 1987.

[MB93] G. Mutschke and U. Bahr. "Kolmogorov-Sinai entropy and Lyapunov spectrum of a one-dimensional Φ^4-lattice model". *Physica D*, 69:302–8, 1993.

[Mei86] J. D. Meiss. "Class renormalization: Islands around islands". *Phys. Rev. A*, 3:2375–83, 1986.

[MO86] J. D. Meiss and E. Ott. "Markov tree model of transport in area-preserving maps". *Physica D*, 20:387–402, 1986.

[Mos62] J. Moser. *Nachr. Akad, Wiss. Goettingen Math.-Phys. K1.2*, 1:1, 1962.

[Nek77] N. N. Nekhoroshev. "An exponential estimate of the time of stability of nearly-integrable Hamiltonian systems". *Russ. Math. Surv.*, 32:1–65, 1977.

[NK95] N. Nakagawa and Y. Kuramoto. "Anomalous Lyapunov spectrum in globally coupled oscillators". *Physica D*, 80:307–16, 1995.

[Pet93] M. Pettini. "Geometrical hints for a nonperturbative approach to Hamiltonian dynamics". *Phys. Rev. E*, 47:828–50, 1993.

[Poi92] H. Poincaré. *"Méthodes Nouvelles de la Mécanique Céleste t.3."*, volume 1. Gauthier-Villars, Paris, 1892. Chapter 5.

[Poi93] H. Poincaré. *"New Methods of Celestial Mechanics"*. American Institute of Physics, 1993. English version of Ref.[Poi92].

[Rue82] D. Ruelle. "Large volume limit of the distribution of characteristic exponents in turbulence". *Comm. Math. Phys.*, 87:287–301, 1982.

[Whi] E. T. Whittaker. *"Analytical Dynamics"*. Chapter 13.

[Yam96] Y. Y. Yamaguchi. "Slow relaxation at critical point of second order phase transition in a highly chaotic hamiltonian system". *Prog. Theor. Phys.* , 95:717–31, 1996.

[Yam97] Y. Y. Yamaguchi. "Second order phase transition in a highly chaotic Hamiltonian system with many degrees of freedom". *International Journal of Bifurcation and Chaos*, 7(4), 1997.

[Yam98] Y. Y. Yamaguchi. "New universality of Lyapunov spectra in Hamiltonian systems". *J. Phys. A*, 1998.

[YK98a] Y. Y. Yamaguchi and T. Konishi. "A geometrical model for stagnant motions in Hamiltonian systems with many degrees of freedom". *Prog. Theor. Phys.*, 1998.

[YK98b] Y. Y. Yamaguchi and T. Konishi. "A geometrical model for stagnant motions in Hamiltonian systems with many degrees of freedom II". *In preparation*, 1998.

[YO87] M. Yamada and K. Ohkitani. "Lyapunov spectrum of a chaotic model of three-dimensional turbulence". *J. Phys. Soc. Jpn.*, 56:4210–3, 1987.

[Yos93] H. Yoshida. "Recent progress in the theory and application of symplectic integrators". *Celestial Mechanics and Dynamical Astronomy*, 56:27–43, 1993.

Index

第 4 章の図表の初出

Yoshiyuki Y. YAMAGUCHI

Slow Relaxation at Critical Point of Second Order Phase Transition in a Highly Chaotic Hamiltonian System

Progress of theoretical physics 95(4), 717-731, 1996-04-25

DOI: 10.1143/PTP.95.717

第 5 章の図表の初出

Yoshiyuki Y Yamaguchi 1998 Journal of Physics A: Mathematical and General 31 195

doi:10.1088/0305-4470/31/1/020

New universality of Lyapunov spectra in Hamiltonian systems

第 6 章の図表の初出

Yoshiyuki Y. YAMAGUCHI and Tetsuro KONISHI

A Geometrical Model for Stagnant Motion in Hamiltonian Systems with many Degrees of Freedom

Progress of theoretical physics 99(1), 139-144, 1998-01-25

DOI: 10.1143/PTP.99.139